# cmgh

ORIGINAL RESEARCH

PGI$_2$ Inhibits Intestinal Epithelial Permeability and Apoptosis to Alleviate Colitis

Camille Pochard,[1] Jacques Gonzales,[1] Anne Bessard,[1] Maxime M. Mahe,[1,2,3] Arnaud Bourreille,[1,4,5] Nicolas Cenac,[6] Anne Jarry,[7] Emmanuel Coron,[1,4] Juliette Podevin,[4] Guillaume Meurette,[1,4] Michel Neunlist,[1] and Malvyne Rolli-Derkinderen[1]

[1]Université de Nantes, Inserm, TENS, The Enteric Nervous System in Gut and Brain Disorders, Institut des Maladies de l'Appareil Digestif, Nantes, France; [2]Department of Pediatric General and Thoracic Surgery, Cincinnati Children's Hospital Medical Center, Cincinnati, Ohio; [3]Department of Pediatrics, University of Cincinnati, Cincinnati, Ohio; [4]CHU de Nantes, Hôpital Hôtel-Dieu, Nantes, France; [5]CIC 1413, Nantes, France; [6]UMR1220, IRSD, INSERM, INRA, INP-ENVT, Université de Toulouse, Toulouse, France; and [7]Université de Nantes, Inserm, CRCINA, Nantes, France
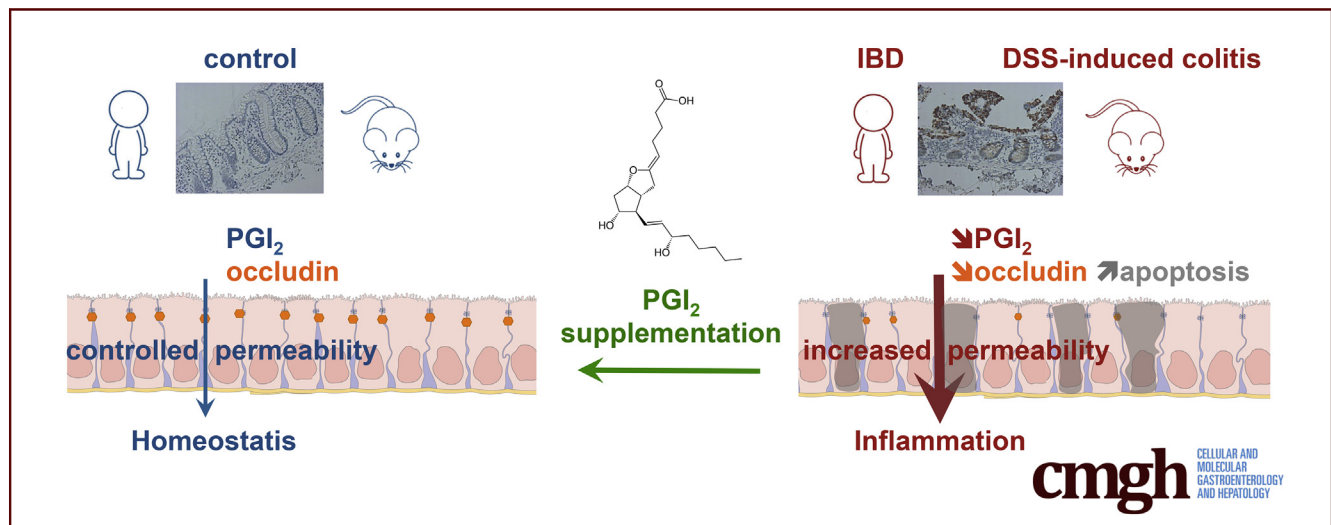
SUMMARY

This study questions reduced prostacyclin production in mucosa from inflammatory bowel disease patients and highlights prostacyclin regulation of the intestinal epithelial barrier. Combining mouse model and human sample analyses, we demonstrated that prostacyclin prevented colitis and occludin down-regulation, inhibited apoptosis, induced occludin membrane location, and reduced intestinal epithelial permeability.

BACKGROUND & AIMS: Inflammatory bowel diseases (IBDs) that encompass both ulcerative colitis and Crohn's disease are a major public health problem with an etiology that has not been fully elucidated. There is a need to improve disease outcomes and preventive measures by developing new effective and lasting treatments. Although polyunsaturated fatty acid metabolites play an important role in the pathogenesis of several disorders, their contribution to IBD is yet to be understood.

METHODS: Polyunsaturated fatty acids metabolite profiles were established from biopsy samples obtained from Crohn's

disease, ulcerative colitis, or control patients. The impact of a prostaglandin I$_2$ (PGI$_2$) analog on intestinal epithelial permeability was tested in vitro using Caco-2 cells and ex vivo using human or mouse explants. In addition, mice were treated with PGI$_2$ to observe dextran sulfate sodium (DSS)-induced colitis. Tight junction protein expression, subcellular location, and apoptosis were measured in the different models by immunohistochemistry and Western blotting.

RESULTS: A significant reduction of PGI$_2$ in IBD patient biopsies was identified. PGI$_2$ treatment reduced colonic inflammation, increased occludin expression, decreased caspase-3 cleavage and intestinal permeability, and prevented colitis development in DSS-induced mice. Using colonic explants from mouse and human control subjects, the staurosporine-induced increase in paracellular permeability was prevented by PGI$_2$. PGI$_2$ also induced the membrane location of occludin and reduced the permeability observed in colonic biopsies from IBD patients.

CONCLUSIONS: The present study identified a PGI$_2$ defect in the intestinal mucosa of IBD patients and demonstrated its protective role during colitis. (Cell Mol Gastroenterol Hepatol 2021;12:1037–1060; https://doi.org/10.1016/j.jcmgh.2021.05.001)

Inflammatory bowel diseases (IBDs) that encompass both ulcerative colitis (UC) and Crohn's disease (CD) are complex chronic inflammatory disorders with increasing incidence and prevalence worldwide in the past decade.[1] IBD is now a major public health problem that affects approximately 3.6 million people in the United States and Europe.[2] IBD is characterized by chronic or relapsing immune activation and inflammation of the gastrointestinal (GI) tract that severely alter its function. Common IBD symptoms include bleeding, severe diarrhea, cramps, abdominal pain, fever, and weight loss. In CD as well as UC, inflammation of the gut is associated with breakdown of intestinal barrier integrity, abnormal secretions, and changes in motility patterns. Despite optimized use of immunosuppressive drugs and development of biotherapies, preventing disease relapse remains a challenge, and surgery is still required in approximately one-third of patients. Failure of approved therapies and in some cases the inability to provide a surgical treatment because of physical extension and/or mislocation of lesions are still major challenges to the management of IBD.[3,4] In the absence of a definitive cure, better understanding of the pathophysiology of IBD is necessary to improve disease outcomes and prevention as well as to discover new effective and lasting treatments.

Although the etiology of IBD has not been fully elucidated, it is currently known that IBD pathogenesis is sustained by aberrant immune responses associated with changes in microbiota composition as well as alterations of the intestinal epithelial barrier (IEB).[5] Numerous susceptibility loci as well as environmental risks factors have been described for CD and UC.[2,6] Despite susceptibility genes that are for the most part different between CD and UC, 30% of IBD-related loci are common to these 2 intestinal diseases. These genes are involved in the immune system modulation, microbiota recognition, and most interestingly in the modulation of IEB functions (permeability, repair, autophagy).[6] IEB-increased permeability has been described as an early feature of IBD,[7,8] and its reduction protects against the development of inflammation.[9] Moreover, increased intestinal permeability has been shown to precede the onset[10] and relapse of CD[11,12] as well as to occur in uninflamed areas.[13] This suggests that intestinal permeability defects can occur irrespective of inflammation. In addition, intestinal mucosal healing is associated with clinical remission.[14,15] Altogether, these events suggest that altered regulation of the IEB might contribute to IBD pathogenesis. Hence, strengthening of the IEB could be part of the therapeutic strategy.

Eicosanoids are potent bioactive signaling lipids derived from arachidonic acid and eicosapentaenoic acid. These polyunsaturated fatty acids (PUFAs) are associated with a diverse set of inflammatory processes linked to various diseases including IBD. The production of some n-6 proinflammatory PUFA derivatives is increased in the lower GI tract of IBD patients compared with control subjects[16–19] or in inflamed mucosa relative to non-inflamed mucosa[20–23] and correlate with inflammation severity.[24] These findings support the idea of an imbalance between the n-6 proinflammatory and n-3 anti-inflammatory derivatives as pathologic contributing factors, but this concept was challenged when it has been found for several derivatives that they could have proinflammatory as well as anti-inflammatory properties.[25–30] In addition, although most PUFA metabolites have been studied individually in an inflammatory context, it has been difficult to get a global view of lipid metabolic cascades that are involved in inflammation-related pathologies. More importantly, recent findings define the importance of pro-resolutive properties of some n-6 derivatives[31] and their homeostatic functions.[32,33] We recently reported that 2 eicosanoids, 15-hydroxyeicosatetraenoic acid (15-HETE) and prostaglandin (PG) 11β-PGF$_{2\alpha}$, can respectively regulate IEB permeability[34] and healing.[35] They are down-regulated in CD,[34,35] suggesting a pro-resolutive and pro-homeostatic function in IBD.

The current study presented a large profile of n-6 and n-3 PUFA-derived bioactive lipid mediators in the supernatant of human biopsies from both IBD and control patients using liquid chromatography coupled to tandem mass spectrometry. Within a cluster of bioactive lipid mediators down-regulated in IBD, PGI$_2$ was identified, and its effects on IEB functions were addressed. In particular, human IEB integrity and colitis development in a mouse model were assessed.

Results

6-ketoPGF$_{1\alpha}$ (PGI$_2$ Metabolite), 11β-PGF$_{2\alpha}$, and PGE$_2$ Are Decreased in Healthy Mucosa From IBD Patients

Using PUFA metabolite profiling from biopsy supernatants, metabolite production was determined in CD (n = 27) or UC (n = 19) versus control (n = 16) patients and in healthy areas (HA) versus unhealthy areas (UHA) in CD and UC patients. Cluster analysis of 23 detected metabolites in biopsy supernatants differentiated 3 clusters of
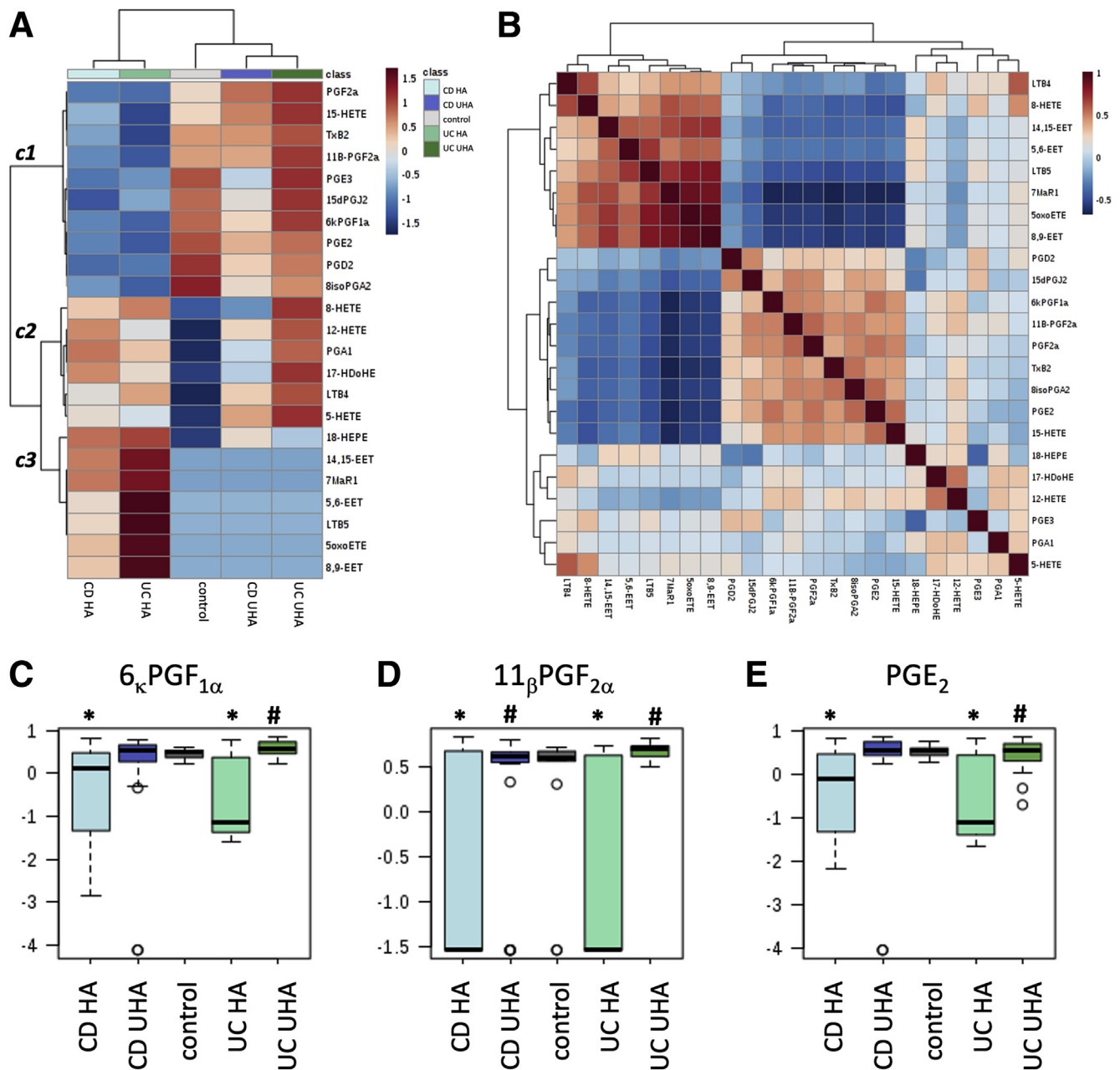
Most current article

Figure 1. *n*-6/*n*-3 PUFA-derived metabolite profiling in biopsy supernatants from control and IBD patients. (*A*) Heatmap of mean concentrations of liquid chromatography-tandem mass spectrometry–identified PUFA metabolites in biopsy supernatants from control patients and HA and UHA of CD and UC patients. Color of each section is proportional to the fold-change of lipids (*red*, up-regulated; *blue*, down-regulated). *Rows*: metabolites; *columns*: patient groups. *c1*, *c2*, *c3* indicate the 3 main clusters identified. (*B*) Correlation analysis of the differential metabolites (*red*, positive correlation factor; *blue*, negative correlation factor). (*C–E*) ANOVA analysis of 6-ketoPGF$_{1\alpha}$ (*C*, stable hydrolyzed product of unstable PGI$_2$), 11β-PGF$_{2\alpha}$ (*D*), and PGE$_2$ (*E*) levels in biopsy supernatants from control and HA and UHA of CD and UC patients. *$P \leq$ .05 versus control; #$P \leq$ .05 UHA versus HA.

metabolites. The first cluster, *c1*, included 10 metabolites down-regulated in HA of CD and UC patients versus UHA and control patients (PGF$_{2\alpha}$, 15-HETE, TxB$_2$, 11β-PGF$_{2\alpha}$, PGE$_3$, 15-deoxyPGJ$_2$, 6-ketoPGF$_{1\alpha}$, PGE$_2$, PGD$_2$, 8-isoPGA$_2$). The second cluster, *c2*, consisted of 6 up-regulated metabolites in HA and UHA of CD and UC patients versus control patients (8-HETE, 12-HETE, PGA$_1$, 17-HDoHE, LTB$_4$, 5-HETE). The last cluster, *c3*, included 7 up-regulated

metabolites in HA of CD and UC patients versus UHA or control patients (18-HEPE, 14,15-EET, 7-MaR1, 5,6-EET, LTB$_5$, 5-oxoETE, 8,9-EET) (Figure 1*A*, Figure 2*A* and *B*). Clustering of lipid profiles was not associated with patient treatments (Figure 3*A* and *B*). This cluster analysis revealed that a cluster of mediators was significantly reduced in HA of IBD patients when compared with control mucosa. Spearman correlation analysis showed a significant
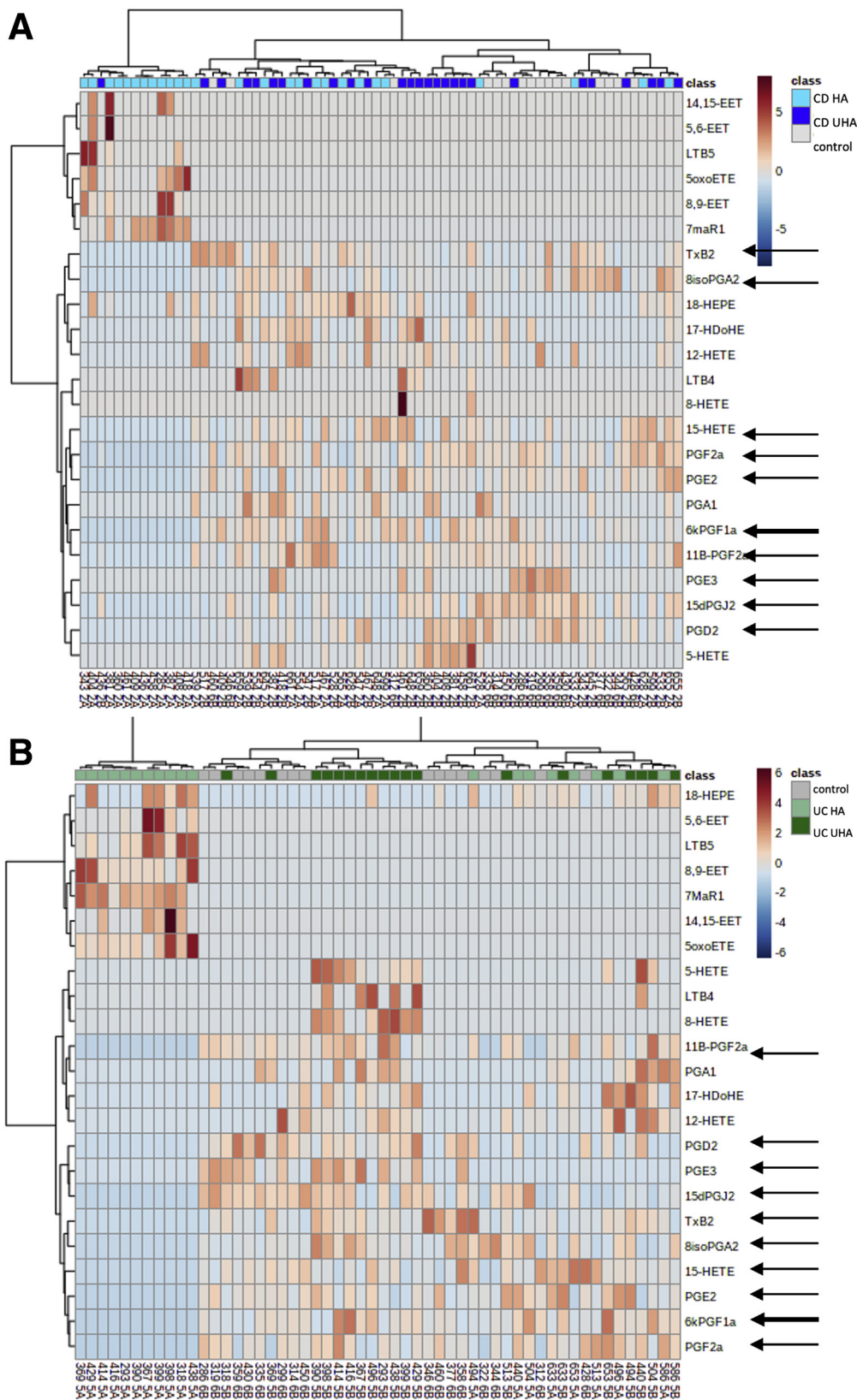
Figure 2. *n*-6/*n*-3 PUFA-derived metabolite profiling in biopsy supernatants from control and IBD patients. (*A*) Heatmap of individual concentrations of liquid chromatography-tandem mass spectrometry–identified PUFA metabolites in biopsy supernatants from control patients (Control) and HA and UHA of CD patients. (*B*) Heatmap of individual concentrations of liquid chromatography-tandem mass spectrometry–identified PUFA metabolites in biopsy supernatants from control patients (Control) and HA and UHA of UC patients. Color of each section is proportional to the fold-change of lipids (*red*, up-regulated; *blue*, down-regulated). *Rows*: metabolites; *columns*: patient identification numbers followed by group identification (2A = CD HA, 2B = CD UHA, 5A = UC HA, 5B = UC UHA, 6B = Control). *Arrows* highlight the metabolites of cluster *c1* identified by analysis of the pool of CD and UC data (Figure 1).

correlation with 9 metabolites from cluster *c1*, excluding only PGE₃ (Figure 1*B*). Interestingly, 5 of 9 correlated metabolites identified in cluster *c1* (15-HETE, 11β-PGF$_{2\alpha}$, 15-deoxyPGJ$_2$, PGD$_2$, PGE$_2$) are known to be involved in IEB integrity, a process that is altered in IBD. Therefore, these 9 mediators from cluster *c1* were focused on. Variance

A

Figure 3. *n*-6/*n*-3 PUFA-derived metabolite profiling in biopsy supernatants from IBD patients according to treatments. (*A*) Heatmap of individual concentrations of liquid chromatography-tandem mass spectrometry–identified PUFA metabolites in biopsy supernatants from HA of CD and UC patients according to their treatments: no treatment (none), anti-tumor necrosis factor (TNF)-α treatment (T), other treatments (o, anti-inflammatory or immunosuppressive drugs), and anti-TNF-α combined with other treatments (To). Color of each section is proportional to the fold-change of lipids (*red*, up-regulated; *blue*, down-regulated). *Rows*: metabolites; *columns*: patient identification numbers followed by group identification (2A = CD HA, 5A = UC HA). (*B*) ANOVA analysis of 6-ketoPGF$_{1\alpha}$ (C, stable hydrolyzed product of unstable PGI₂) concentrations in biopsy supernatants from control untreated patients (CONT none) and CD and UC patients without treatment (none), treated with anti-TNF-α, anti-inflammatory, or immunosuppressive drugs (others), and anti-TNF-α combined with other treatments (anti-TNF-α and others).

B
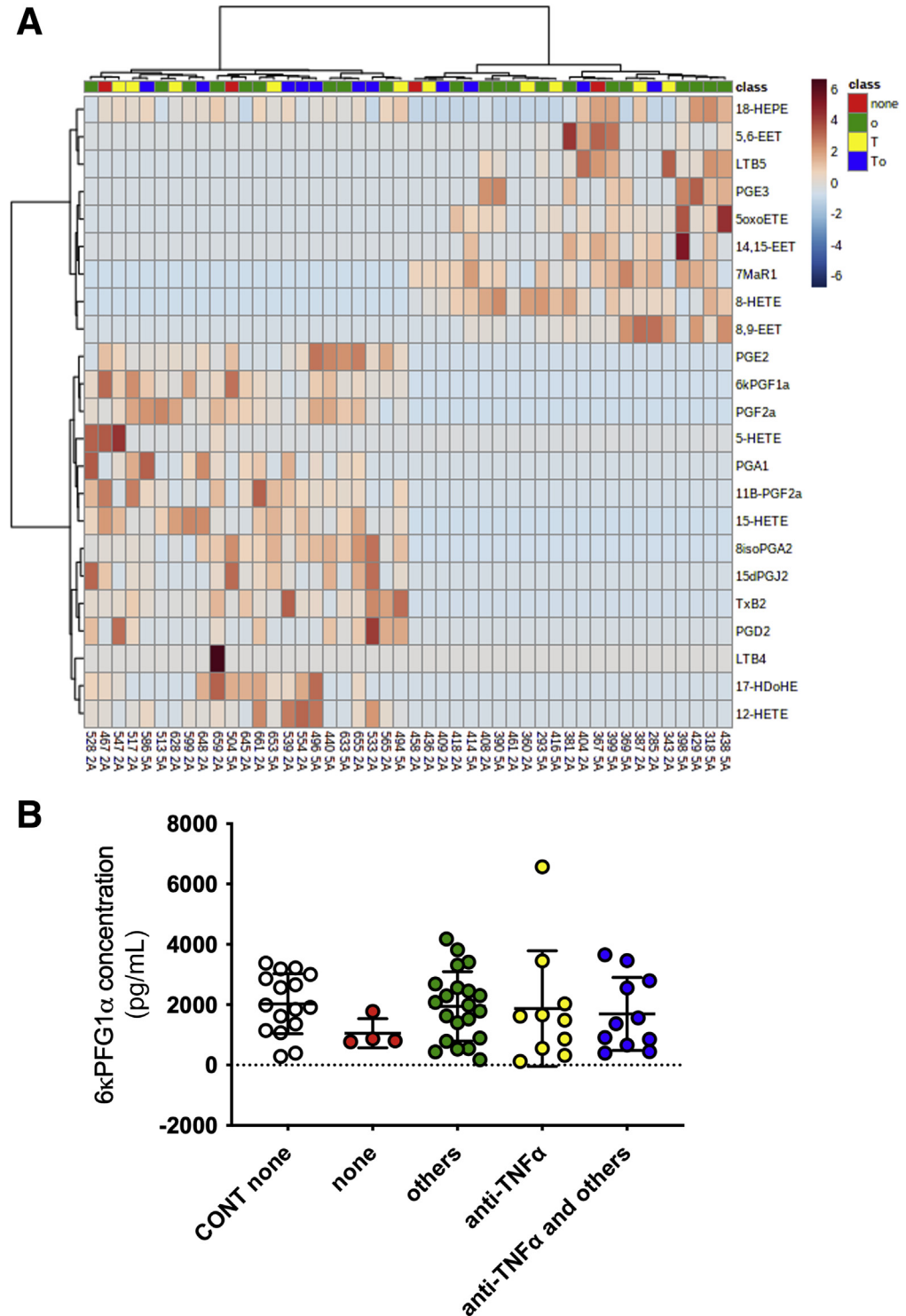
analyses demonstrated that the concentrations of 6-ketoPGF$_{1\alpha}$ (Figure 1*C*), 11β-PGF$_{2\alpha}$ (Figure 1*D*), and PGE₂ (Figure 1*E*) were significantly lower in HA of CD or UC patients compared with control patients. In addition, their concentrations were significantly increased in UHA versus HA for UC patients (Figure 1*C–E*). Although 11β-PGF$_{2\alpha}$ and PGE₂ involvement in IEB regulation has been described,[35,36] the role of PGI₂ (6-ketoPGF$_{1\alpha}$ is the stable, inactive metabolite of the bioactive PGI₂) is yet to be known. Thus, focus was centered on PGI₂ regulation of

intestinal permeability and its putative role in IEB defects observed in IBD patients.

PGI₂ Decreases Caco-2 Monolayer Permeability

To investigate PGI₂ effects on IEB, whether the PGI₂ analog iloprost can directly modulate the resistance and permeability of Caco-2 intestinal epithelial cell (IEC) monolayers in vitro was assessed. This PGI₂ analog significantly increased the transepithelial electrical resistance

(TEER) (Figure 4A) and decreased paracellular permeability of Caco-2 monolayers compared with untreated cells (Figure 4B). Iloprost significantly regulated permeability when applied to the basolateral but not when applied to the apical side (Figure 4J).[37] To ensure that the observed effects were not mediated by the inactive PGI_2 degradation product 6-ketoPGF$_{1\alpha}$, the TEER and permeability of Caco-2 cells treated with 6-ketoPGF$_{1\alpha}$ were also measured. Both TEER (Figure 4K) and permeability (Figure 4L) remained unchanged. These data demonstrate that PGI_2 can directly regulate IEB resistance and permeability.

PGI_2 Increases Occludin and Decreases Claudin-2 and Zonula Occludens-1 Expression In Vitro

To investigate the mechanisms of PGI_2 regulation of IEB permeability, expression of tight junction proteins and regulators of paracellular permeability in Caco-2 cells treated or untreated with iloprost was assessed. Zonula occludens-1 (ZO-1) and claudin-2 expression were significantly decreased in the presence of iloprost (Figure 4C–E). In contrast, occludin expression was significantly increased by iloprost treatment (Figure 4C and F). Junctional adhesion molecule-A, cingulin, and phosphorylated myosin light chain (MLC) 20 expressions were unchanged by iloprost treatment (Figures 4C and G–I). These data showed that PGI_2 analog treatment modified tight junction protein expression.

PGI_2 Inhibits Dextran Sulfate Sodium–Induced Colitis and Prevents Increased Permeability and Mucosal Destruction In Vivo

To study the role of PGI_2 in vivo, the damage observed in dextran sulfate sodium (DSS)-induced mouse colitis model was examined with or without synthetic PGI_2 epoprostenol treatment (Figure 5A). The typical weight loss observed in DSS-induced mice was absent when they received PGI_2 (Figure 5B). As expected, the Disease Activity Index (DAI), which considers stool consistency and gross bleeding, significantly increased in DSS-induced mice compared with control animals and significantly decreased in PGI_2-treated mice compared with DSS-induced colitis mice (Figure 5C). To assess the impact of PGI_2 supplementation on IEB integrity, intestinal permeability was measured in vivo. Paracellular permeability was increased in DSS-induced mice compared with control animals, and PGI_2 treatment reduced the DSS-induced permeability to baseline levels (Figure 5E). Transcellular permeability was unaffected between all 4 experimental groups (Figure 5D). Both the cecal atrophy and reduction of colon length observed in DSS-treated mice were prevented when these mice simultaneously received PGI_2 (Figure 3F and G). Epoprostenol injections in control mice did not affect the measured parameters (Figure 3B–G). The DSS-induced changes in distal colon morphology were also prevented by PGI_2 treatment (Figure 5I). Quantification of this intestinal remodeling showed that PGI_2 treatment prevented mucosal architecture alteration (Figure 5H) but did not prevent muscle thickening (Figure 5J). Mucosal infiltration by immune cells and goblet cell depletion were only significantly increased in DSS-induced colitis mice compared with control mice without PGI_2 treatment (Figure 5K and L). Altogether, these data showed a beneficial role of PGI_2 supplementation that prevented intestinal damage observed in vivo during colitis development induced by DSS.

PGI_2 Partially Reduces Inflammation Observed in DSS-Induced Colitis

The effect of PGI_2 on the colonic inflammatory response induced by DSS with or without synthetic PGI_2 epoprostenol treatment was investigated next. DSS-induced increases in tumor necrosis factor-α (Figure 6A), interleukin (IL) 6 (Figure 6C), and IL17A (Figure 6E) mRNA expression were not affected by PGI_2 treatment. In contrast, DSS-induced increases in IL1β (Figure 6B), interferon (IFN-γ) (Figure 6D), and IL22 (Figure 6F) mRNA expression were not significant when animals were treated with PGI_2. These data suggested that PGI_2 partially tampers with the inflammatory process via down-regulation of cytokines such as IL22, IFN-γ, and IL1β.

PGI_2 Protects Against DSS-Induced Decreases in Occludin Expression and Apoptosis

To investigate the molecular remodeling associated with PGI_2 effects on IEB during colitis development, expressions of occludin and claudin-2, the 2 tight junction proteins identified in Caco-2 cells (Figure 4), were analyzed in mice colons. Occludin immunostaining showed clear epithelial staining unchanged by PGI_2 supplementation. DSS-induced colitis decreased occludin staining that was restored by PGI_2 treatment (Figure 7A and C). Because IEB permeability could be regulated by changes in tight junction protein expression as well as modulation of IEC apoptosis or renewal, cleaved caspase-3 expression, proliferating cell nuclear antigen (PCNA) expression, and Akt phosphorylation in the colon of DSS-induced mice with or without PGI_2 treatment were measured. Immunofluorescent staining revealed a higher level of cleaved caspase-3 in the colonic mucosa of DSS-induced colitis mice compared with controls, mice treated with PGI_2 alone, and DSS-induced mice treated with PGI_2 (Figure 7B and D). PCNA expression was not modified (Figure 7E and F), but Akt phosphorylation was increased in DSS-induced mice treated with PGI_2 compared with PGI_2-treated animals (Figure 7E and G). These data suggested that in addition to maintenance of occludin expression, PGI_2 can play an epithelial protective role by decreasing apoptosis and promoting IEC survival.

PGI_2 Inhibits Apoptosis and Permeability and Induces Membrane-Associated Occludin Expression in Human and Mouse Explants Ex Vivo

To validate PGI_2 ability to prevent IEB permeability induced by altered tight junction proteins and epithelial apoptosis, colonic samples from control mice and mucosal explants from control patients treated with the apoptosis inducer staurosporine were treated with or without iloprost, and permeability was measured in Ussing chambers. Mice
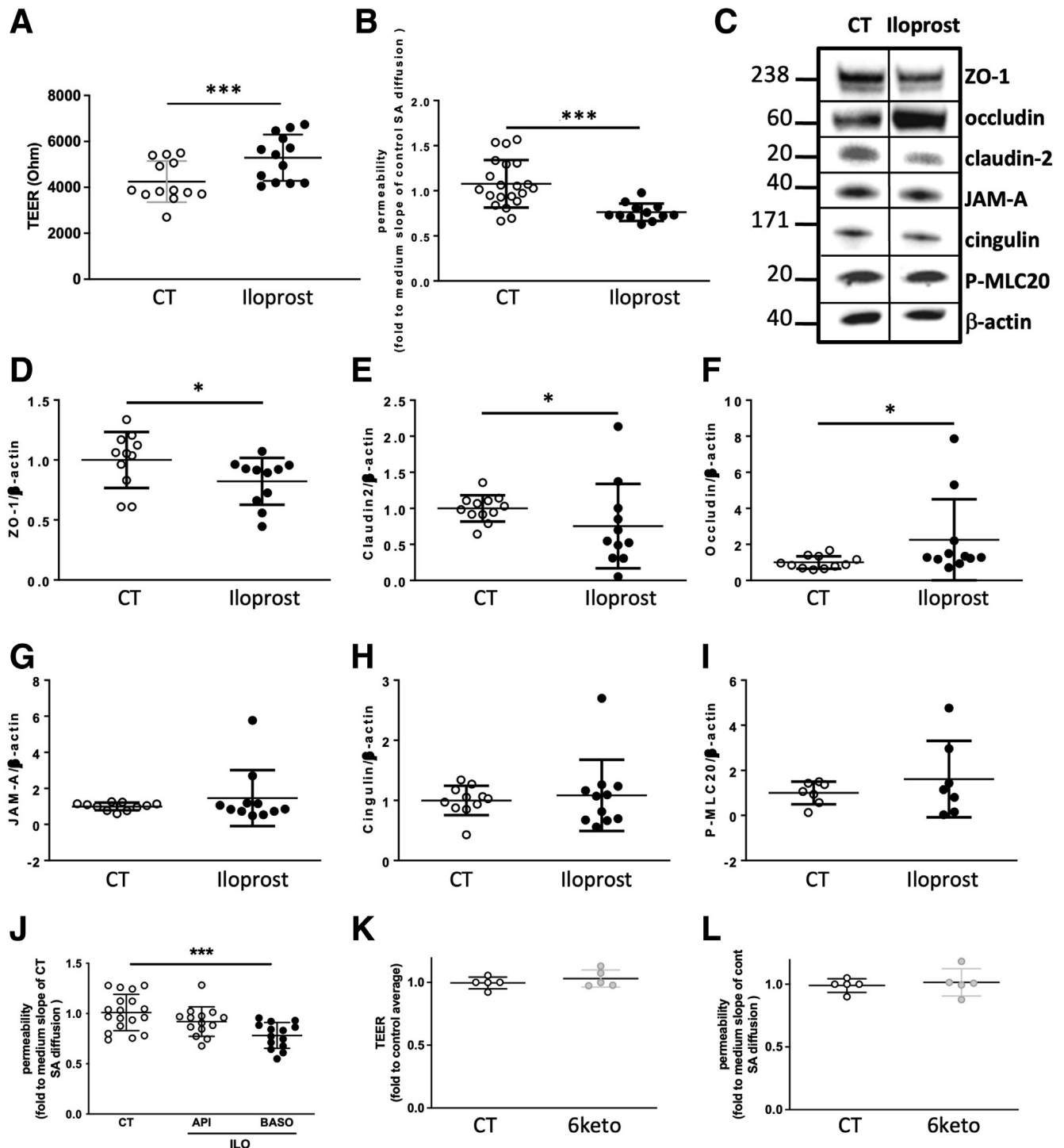
Figure 4. PGI$_2$ analog iloprost increases resistance, reduces permeability, increases occludin, and decreases ZO-1 and claudin-2 expression in vitro. (*A* and *B*) PGI$_2$ impact on TEER (*A*) and permeability (*B*) was measured in vitro on Caco-2 monolayer after 1 day with or without (CT) 10 μmol/L iloprost in the basolateral compartment. Data represent means ± SEM of 13–16 Caco-2 filters per condition. ***$P < .001$ Mann-Whitney test. (*C–I*) Western blot analyses of tight junction protein expression from Caco-2 lysates. Representative Western blot (*C*), ZO-1 (*D*), claudin-2 (*E*), occludin (*F*), junctional adhesion molecule-A (*G*), cingulin (*H*), and phosphorylated MLC20 (*I*) expression quantification related to β-actin expression from Western blot analysis. In (*D–I*), data represent means ± SEM of 7–12 Caco-2 filters per condition. *$P \leq .05$ nonparametric Mann-Whitney test. (*J*) Sulfonic acid permeability was measured on Caco-2 monolayer after 1 day of 10 μmol/L iloprost (ILO) treatment in basolateral (Baso) or apical (Api) compartments or without it (Cont). (*K*) TEER was measured on Caco-2 monolayer after 1 day of 10 μmol/L 6-ketoPGF$_{1\alpha}$ (6 keto) treatment in the basolateral compartment or without it (Cont). (*L*) Paracellular permeability was measured by sulfonic acid (SA) flux through the same Caco-2 monolayer. Data represent means ± SEM of 3–6 independent experiments. *$P > .05$ by nonparametric Mann-Whitney test.

explants treated with staurosporine showed an increased cleaved caspase-3 level and apoptosis score (Figure 8A and D) associated with a decrease in occludin expression (Figure 8B), mucosal architecture disorganization (Figure 8C), and

increased permeability (Figure 8E). Supplementation with the PGI$_2$ analog iloprost prevented all these changes (Figure 8A–E). Dose-response experiments demonstrated that 1 μmol/L iloprost had no significant effect (Figure 9A).
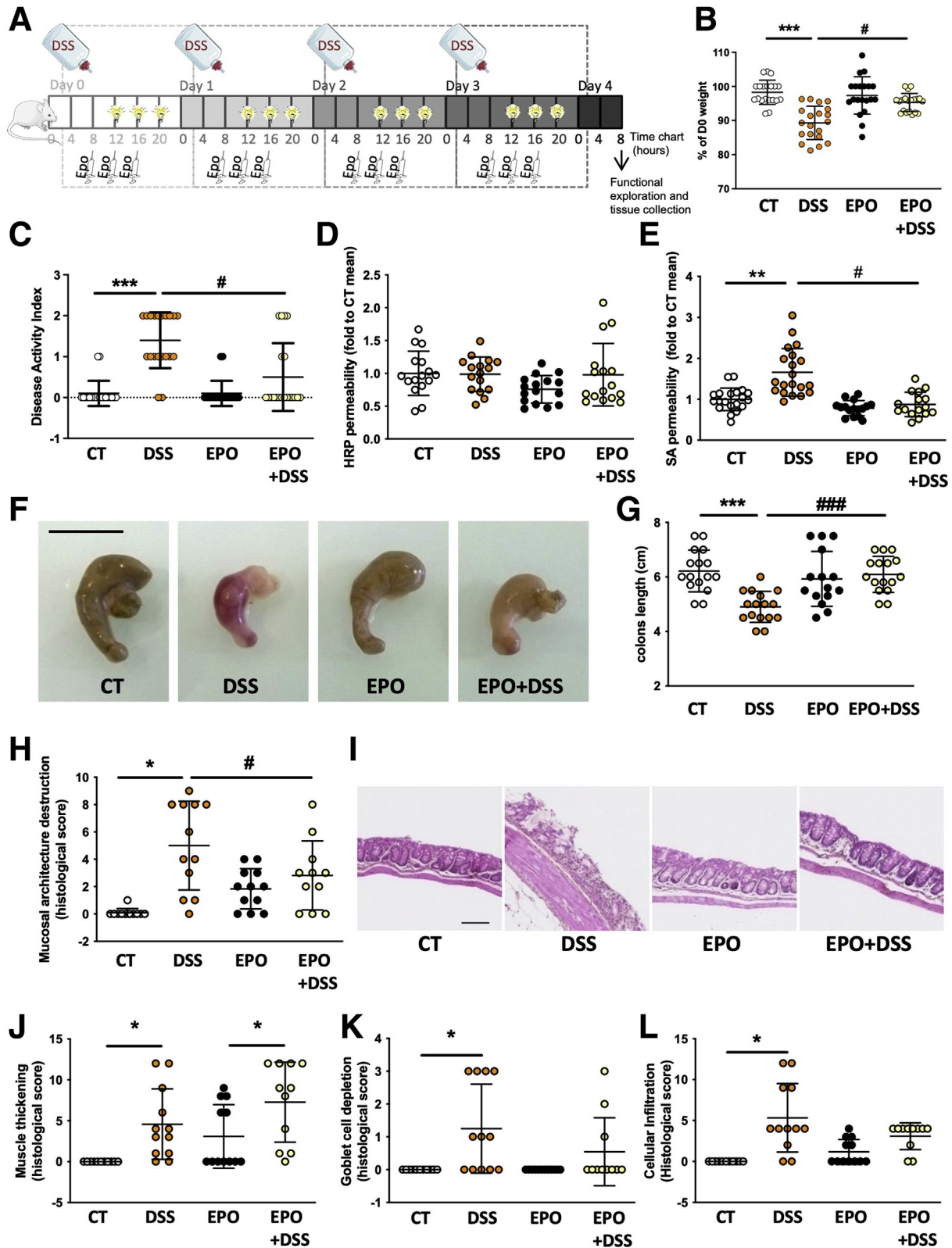
Cell fractionation analyses showed that rather than an increase in total occludin expression, iloprost increased membrane-associated occludin (Figure 9B and C). In human explants, staurosporine treatment also increased paracellular permeability that was entirely inhibited by iloprost supplementation, leading to a recovery of permeability values (Figure 10A). Altogether, these data demonstrated that iloprost was able to prevent apoptosis-induced permeability. Cleaved caspase-3 expression increased within 2–5 hours after staurosporine treatment. This effect was again entirely inhibited by iloprost pretreatment (Figure 10B).

Apoptosis and Cleaved Caspase-3 Expression Are Increased in the Mucosa of CD and UC Patients

To determine whether apoptosis was increased in the mucosa of IBD patients, apoptosis was measured by (1) immunohistochemistry using an antibody directed to cleaved caspase-3 or the cytodeath M30 antibody specific for apoptotic epithelial cells[38] and (2) measuring BAX and BCL2 mRNA expression in the mucosa of control, CD, and UC patients. Whereas the expression of cleaved caspase-3 was increased in CD and UC patients compared with control patients (Figure 10C and D), BCL2 and BAX mRNA were unchanged (Figure 10E and F). Immunohistochemistry of cleaved caspase-3 and epithelial apoptosis measurement using cytodeath M30 showed very low levels of cleaved caspase-3$^+$ or cytodeath M30$^+$ cells in control patients, whereas high numbers of both were observed in CD or UC patients (Figure 10C). These data indicate that epithelial apoptosis was increased in the mucosa of CD and UC patients compared with control patients. To determine how tight junction proteins are expressed in biopsies from IBD patients and whether it is dependent on disease activity, ZO-1 and occludin expressions in biopsies from control, quiescent, or active (HA and UHA) CD patients were analyzed. Whereas ZO-1 expression was not significantly altered (Figure 10H), occludin expression was significantly decreased in UHA of CD patients compared with HA or control biopsies (Figure 10I).

PGI₂ Reduces Permeability of Biopsies From IBD Patients

To assess whether PGI₂ treatment can reduce the increased permeability observed in IBD patients, biopsies from CD or UC patients were pretreated with the PGI₂ analog iloprost 1 hour before paracellular permeability measurement in Ussing chambers. Iloprost treatment significantly decreased the permeability of IBD biopsies (Figure 11A). This decrease was not due to altered expression of ZO-1 or occludin (Figure 11B) or the PGI₂ receptor (IP) in the mucosa of IBD patients because IP mRNA levels were not significantly different in CD or UC versus control mucosa (Figure 9G). Nevertheless, cell fractionation and immunohistochemistry analyses showed that occludin membrane expression increased when biopsies were treated with iloprost (Figure 11C–E). These results showed that PGI₂ can reduce the permeability of IBD biopsies, suggesting that the functional defect of PGI₂ mucosal production by IBD patients could be fixed by addition of a PGI₂ analog.

Discussion

Whereas IEB integrity loss is a well-recognized IBD contributing factor,[39] the underlying molecular mechanisms of IEB failure and strategies dedicated to protect and/or improve IEB remain to be identified. Not only does the current work give a clear picture of lipid metabolic profiles in human samples and better define the role of PGI₂ in IEB homeostasis, it also aids the understanding of n-6 PUFA-metabolite contributions to IBD development and proposes its use as an IEB reinforcing agent in IBD.

Our current findings first highlight a cluster of n-6 PUFA metabolites that are less present in supernatants of HA from CD or UC patients compared with UHA or control patients. This cluster is composed of 4 principal bioactive PGs (PGD₂, PGE₂, PGF$_{2\alpha}$, PGI₂), 2 PGD₂ metabolites (11β-PGF$_{2\alpha}$, 15-deoxyPGJ₂), thromboxane A2, and 1 eicosanoid (15-HETE). It is important to note that their concentrations are decreased in non-inflamed HA but increased in inflamed UHA, which is consistent with the increased PG production generally induced by acute inflammation[40] and already observed in rectal mucosa of active UC patients,[19,41,42] inflamed esophageal mucosa,[43] or experimental ileitis.[44] Nevertheless, genome-wide analysis of DNA methylation identified the down-regulation of the PGI₂ synthase in fibrotic CD patients,[45] reinforcing the idea that the decrease in PGI₂ content observed in HA of CD or UC patients herein could sensitize IEB and participate in IBD development.

The deleterious effect of PG defects reported in studies using PG inhibition has long been described in intestinal mucosa, not in IBD but through observations of gastric mucosal erosion and small intestine lesions induced by

---

Figure 5. (*See previous page*). **Synthetic PGI₂ epoprostenol prevents DSS-induced colon atrophy, animal weight loss, and mucosal destruction and increases permeability in vivo.** (A–E) PGI₂ impact on colitis induced by DSS in vivo was measured at end of the protocol in control (CT) or DSS-induced mice (DSS) that received PBS (NT) or epoprostenol (EPO) during the 4 days of the protocol. Experimental design (A), animal weight (B), DAI (C), transcellular permeability (D), and paracellular permeability (E) (evaluated by measurement of HRP and sulfonic acid in animal plasma 4 hours after mouse gavage), cecal remodeling (F; scale bar: 1 cm), and colon length (G). (H–L) Tissue remodeling was analyzed in the 4 groups of mice. Hematein Phloxin Safran coloration of distal colon sections of control (CT), DSS-induced (DSS), epoprostenol-treated (EPO), or epoprostenol-treated DSS-induced (EPO+DSS) mice (I; scale bar: 100 μm). Histologic scores were evaluated from Hematein Phloxin Safran staining by quantifying the destruction of mucosal architecture (H), muscle thickening (J), loss of goblet cells (K), and cellular infiltration (L). Data represent mean ± SEM of 4–12 mice per group. Two-way ANOVA followed by Bonferroni post hoc tests. *$P \leq .05$, **$P \leq .01$ and ***$P \leq .001$ (DSS factor effects) or #$P \leq .001$ and ###$P \leq .001$ (EPO factor effects).
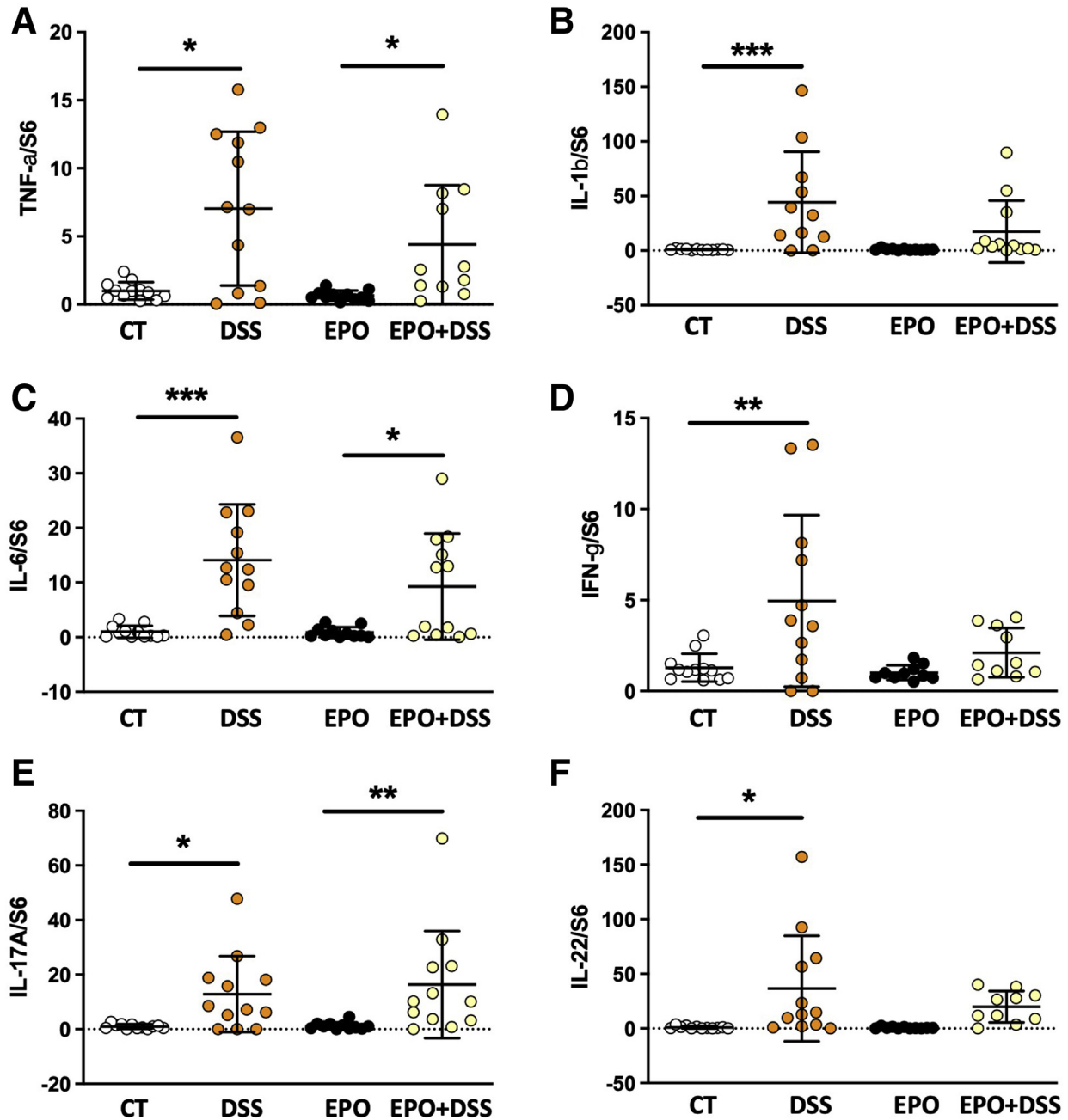
Figure 6. Synthetic PGI$_2$ epoprostenol partially prevents inflammation observed during colitis development. (A–F) mRNA expression of tumor necrosis factor (*Tnf*)-α (A), *IL-1β* (C), *IL-6* (C), *IFN-γ* (D), *IL-17A* (E), and *IL-22* (F) was measured at end of 4-day treatment in colon fragments of control (CT) or DSS-induced mice (DSS) that received PBS (NT) or epoprostenol (EPO) every day. Data represent means ± SEM of 12 mice per group. Two-way ANOVA followed by Bonferroni post hoc tests. *$P \leq$ .05, **$P \leq$ .01, and ***$P \leq$ .001 (DSS factor effects).

cyclooxygenase inhibition.[46] A decrease in endogenous gastric prostanoid synthesis has also been observed in ulcers,[47–49] and the beneficial impact of PG supplementation on intestinal mucosa was described in the 1980s, particularly through the concept of cytoprotection developed by André Robert. He and others described how PG can prevent induction of gastric mucosal erosion and mainly concerns PGE$_2$.[50,51] Numerous works have described PGE$_2$ effects in the GI tract, driving the current idea that PGE$_2$-specific

effects depend on the targeted receptor (EP1–4) and cell type and could provide mucosal protection to colitis trough EP4/2 receptors.[36,52,53] Concerning PGD$_2$, how its metabolites, 11β-PGF$_{2\alpha}$ and 15-deoxyPGJ$_2$, increase IEB healing[35] and modulate epithelial cell proliferation and differentiation has already been described.[54] Nevertheless, the role of PGD$_2$ in gut inflammation remains debated since Hokari et al[27] suggested that *L*-PGD synthase plays a proinflammatory role in the development of colitis in clinical and

experimental studies. On the other hand, PGD$_2$/DP1 axis activation has been shown to confer anti-inflammatory properties[26,29] and reduce colitis development.[28]

As for the other PG, PGI$_2$'s impact on gut function is manifold and complex because it regulates and is produced by different cell types, but its regulation of IEC function is not well-described. Indeed, we know that PGI$_2$ regulates

gastric emptying and small intestinal transit[55] through regulation of smooth muscle contraction.[56–59] PGI$_2$ is a well-known vasodilator,[60] inhibitor of platelet aggregation,[61] and promoter of angiogenesis,[62] and it is precisely through these vascular effects that PGI$_2$ has a remarkable action against anastomotic leakage under artificially obstructive conditions,[63] could enhance colon anastomotic healing,[64] or
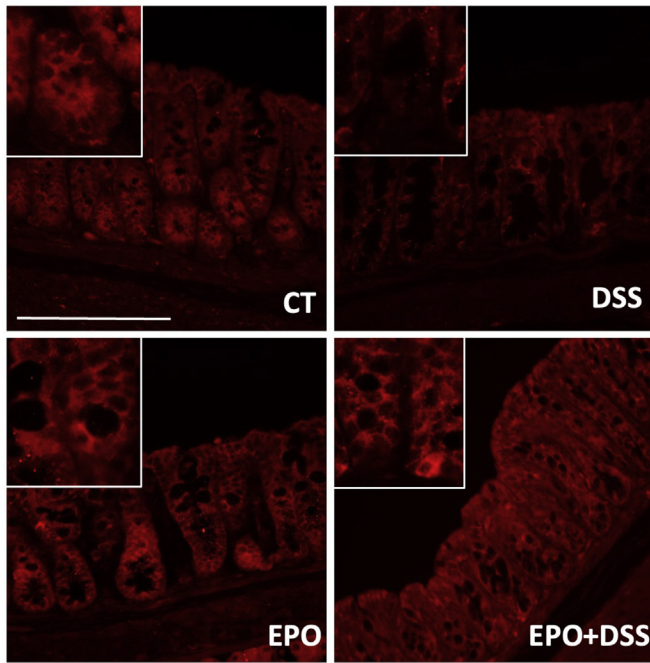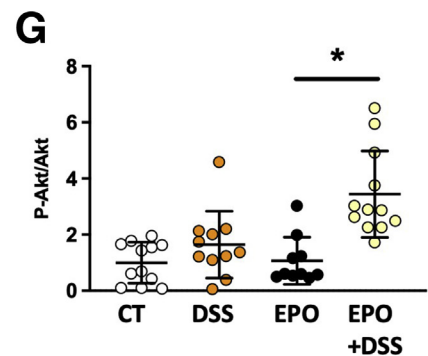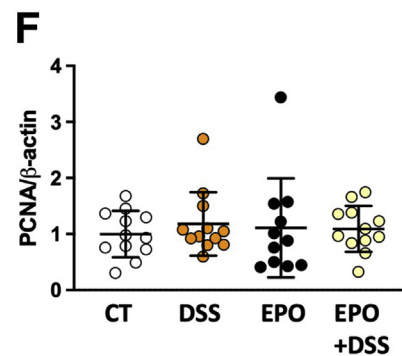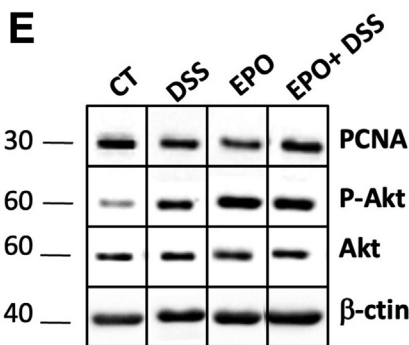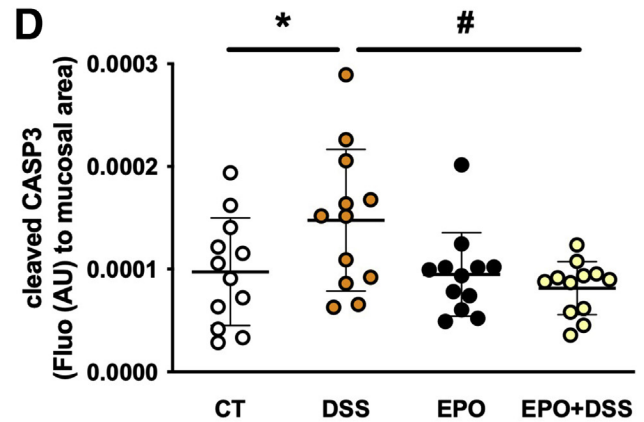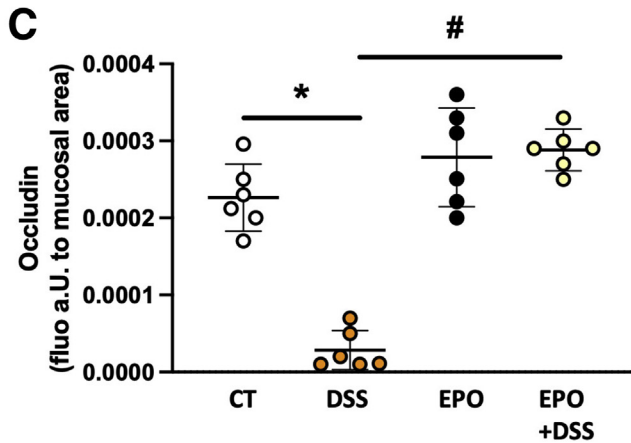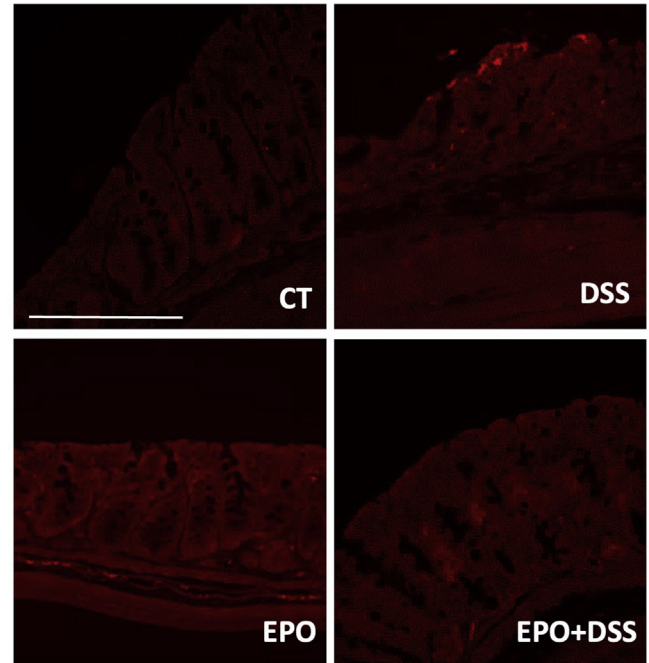
improve intestinal barrier function.[65] Its well-described impact on the IEB itself includes reduction of acid secretion,[66,67] induction of chloride secretion,[68,69] and inhibition of water and solute absorption.[70,71] Concerning PGI_2 regulation of IEC proliferation or apoptosis, studies are contradictory. PGI_2 promotes HT29 cell proliferation in vitro[72] but does not stimulate growth of gastroduodenal mucosa in vivo.[67] It does not impact HT29 apoptosis[72] but promotes colonocyte survival and presents some anti-apoptotic effects through peroxisome proliferator-activated receptor δ activation.[73] A working hypothesis is that these effects participate in the increased restitution of IEC6 or Caco-2 cells[74] and increased IEB restoration and resistance induced by PGI_2 when paired with PGE_2.[75–78]

Our present work provides evidence that PGI_2 regulates intestinal epithelial permeability as well as tight junctions and has anti-apoptotic properties. We demonstrated that in vitro treatment of intestinal epithelial monolayers or isolated mouse or human mucosa explants with the PGI_2-stable analog iloprost decreases IEB permeability, increases occludin membrane expression, and protects against apoptosis. These effects could have been attributed to the activation of other eicosanoid pathways, because iloprost is not entirely selective for the PGI_2 receptor (IP) but could activate PGE_2 EP1–4 receptors.[79] Nevertheless, similar effects were found using the synthetic PGI_2 epoprostenol, which can activate EP3 and more specifically the IP.[80] Indeed, the present study demonstrated that PGI_2 supplementation in vivo inhibits DSS-induced colitis by decreasing induced epithelial permeability, maintaining occludin expression, and inhibiting epithelial apoptosis. Altogether, our findings show that PGI_2 is able to strengthen the IEB and suggest that this strengthening contributes to alleviation of colitis in vivo.

Interestingly, the IEB properties improved by PGI_2 are deficient in IBD patients in whom increased permeability has been explained by defects in tight junction function or IEC renewal. In CD as well as UC, claudin-2 up-regulation, MLC kinase activation, or occludin down-regulation have already been observed.[81] In addition to the regulation of permeability by tight junction proteins that occurs when the epithelium is intact, epithelial cell death can also cause barrier loss regardless of tight junction function.[82] It has already been shown that lipopolysaccharide-induced apoptosis causes an increase in IEB paracellular permeability[83] and that cleaved caspase-3 is associated with increased permeability in other colitis models.[84] After 4 days of DSS treatment, an increase in cleaved caspase-3 expression in the colon of the current colitis-mouse model was observed. This cleavage is consistent with the increase in cleaved caspase-3 observed in tissues from IBD patients that also presented higher epithelial apoptosis. Because changes in *BCL2* or *BAX* mRNA expression in the mucosa of CD or UC patients were not observed herein, it could be hypothesized that the transduction pathway leading to apoptosis is mainly an extrinsic one concerning IEC death receptor pathway activation. Moreover, the PGI_2 analog iloprost was demonstrated to efficiently inhibit apoptosis-induced permeability as well as permeability observed in IBD patient biopsies. This strongly suggests that the functional defect of PGI_2 mucosal production in IBD patients could be fixed by additional treatment with a PGI_2 analog.-Whereas PGI_2 involvement in IEB homeostasis and functions was sparse, our work identified a decrease in PGI_2 content in intestinal mucosa from IBD patients and clearly demonstrated that PGI_2 can directly target the IEB to decrease apoptosis and colitis-induced IEB permeability. In addition, the observation that PGI_2 supplementation decreased cellular infiltration as well as *IL22* and *IL1β* expression in vivo in the DSS-induced colitis model suggests a more global modulatory effect of PGI_2, not only on epithelial but also on immune homeostasis. This idea is supported by the link and common mechanisms between IBD and chronic airway diseases[85] and the current widespread use of stable PGI_2 analogs beraprost and iloprost as treatment for pulmonary hypertension. These analogs showed potent anti-inflammatory and endothelium-dependent anti-edemagenic effects in several models of acute lung injury.[86] Nevertheless, investigation of PGI_2 supplementation impact on immune cells and vascular functions remains to be completed before considering whether targeting the PGI_2 pathway may be therapeutically relevant in IBD.

Methods
Study Approval

Patients provided written informed consent to take part in the study, and all procedures were performed according to the guidelines of the French Ethics Committee for

Figure 7. (*See previous page*). Synthetic PGI_2 epoprostenol inhibits decreased occludin expression and apoptosis induced by DSS in vivo. (*A* and *C*) PGI_2 impact on occludin expression. Representative occludin immunostaining of distal colon sections of control (CT), DSS-induced (DSS), epoprostenol-treated (EPO), or epoprostenol-treated and DSS-induced (EPO+DSS) mice at end of 4-day treatment (*A*; scale bar: 100 μm). Occludin mucosa staining was quantified in the 4 groups of mice (*C*). (*B* and *D*) PGI_2 impact on apoptosis. Representative cleaved caspase-3 immunostaining of distal colon sections of control (CT), DSS-induced (DSS), epoprostenol-treated (EPO), or epoprostenol-treated and DSS-induced (EPO+DSS) mice at end of 4-day treatment (*B*). Quantification of cleaved caspase-3 staining relative to mucosal area in the 4 groups of mice (*D*). Data represent means ± SEM of 4 mice per group. Two-way ANOVA followed by Bonferroni post hoc tests. *$P < .05$ (DSS factor effects) or #$P < .05$ (EPO factor effects). (*E–G*) Western blot analyses of PCNA, phospho-Akt (P-Akt), and Akt were performed on the distal colon of control (CT), DSS-induced (DSS) epoprostenol-treated (EPO), or epoprostenol-treated and DSS-induced (EPO+DSS) mice at end of 4-day treatment. Representative Western blot analysis of PCNA and P-Akt/Akt expression (*E*). Quantification of PCNA expression (*F*). Quantification of P-Akt/Akt expression derived from acquisition of the same gels (*G*). Data represent means ± SEM of 12 mice per group. Two-way ANOVA followed by Bonferroni post hoc tests. *$P \leq .05$ (DSS factor effects) or #$P \leq .05$ (EPO factor effects).
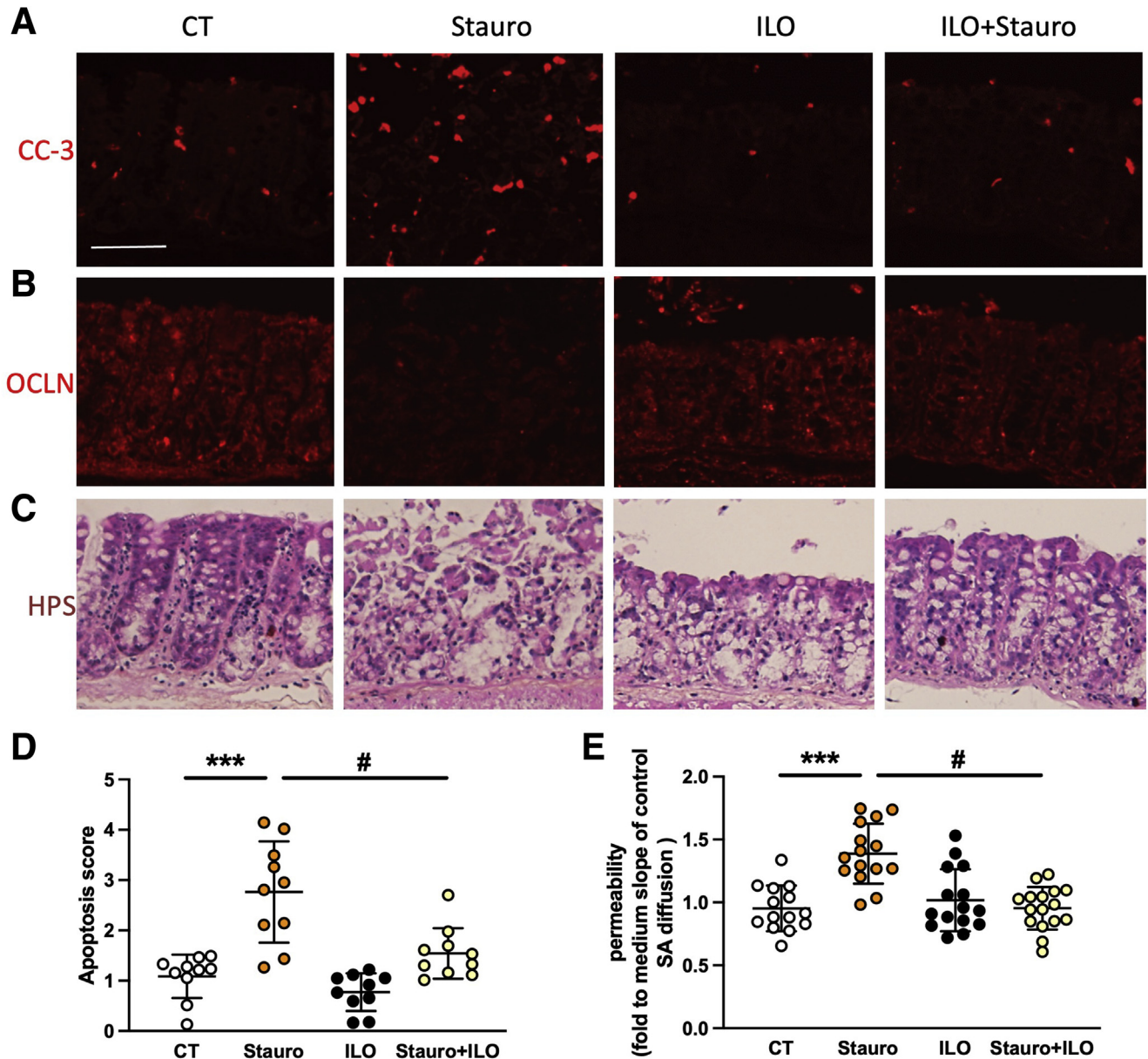
Figure 8. PGI$_2$ analog iloprost prevents mouse IEB breakdown ex vivo. (*A–D*) Potential of PGI$_2$ to block IEB breakdown induced by apoptosis was assessed on mouse colon explants treated without (CT) or with staurosporine (Stauro, 1 μmol/L) for 20 hours, without or with 4-hour pretreatment with 10 μmol/L iloprost pretreatment (ILO). Representative cleaved caspase-3 (CC3, *A*), occludin (OCLN, *B*), or Hematein Phloxin Safran staining (HPS, *C*) of explants from proximal colon of mice after the mentioned treatments (scale bar: 50 μm). Apoptosis score evaluated from cleaved caspase-3 staining (*D*). Paracellular permeability measured in Ussing chambers by sulfonic acid flux through mouse tissues after the mentioned treatments (*E*). Data represent means ± SEM of 16 explants per group. Two-way ANOVA followed by Bonferroni post hoc tests. ***$P \le .001$ (for DSS factor effects) or #$P \le .05$ (for ILO factor effects).

Research on Humans and registered under no. DC-2008-402. All experiments involving mice were approved by the Ethics Committee for Animal Experimentation of Pays de la Loire (study no. 01953.01).

Patients

Human tissues originating from control, CD, or UC patients were used for biopsy supernatant analyses (Table 1), mucosa explants (Table 2), mucosa histology, molecular analyses (Table 3), and biopsy permeability analyses (Table 4). Briefly, surgical resections (used for explants and mucosa analyses) were collected from macroscopically and microscopically unaffected fragments from patients undergoing surgery. Control patients were those undergoing surgery for colon cancer except 2 who were undergoing surgery for stenosis or Hartmann's procedure that were used for explants. Samples were always taken at least 10 cm away from the tumor. Biopsies were taken in macroscopically UHA and/or HA. Whereas
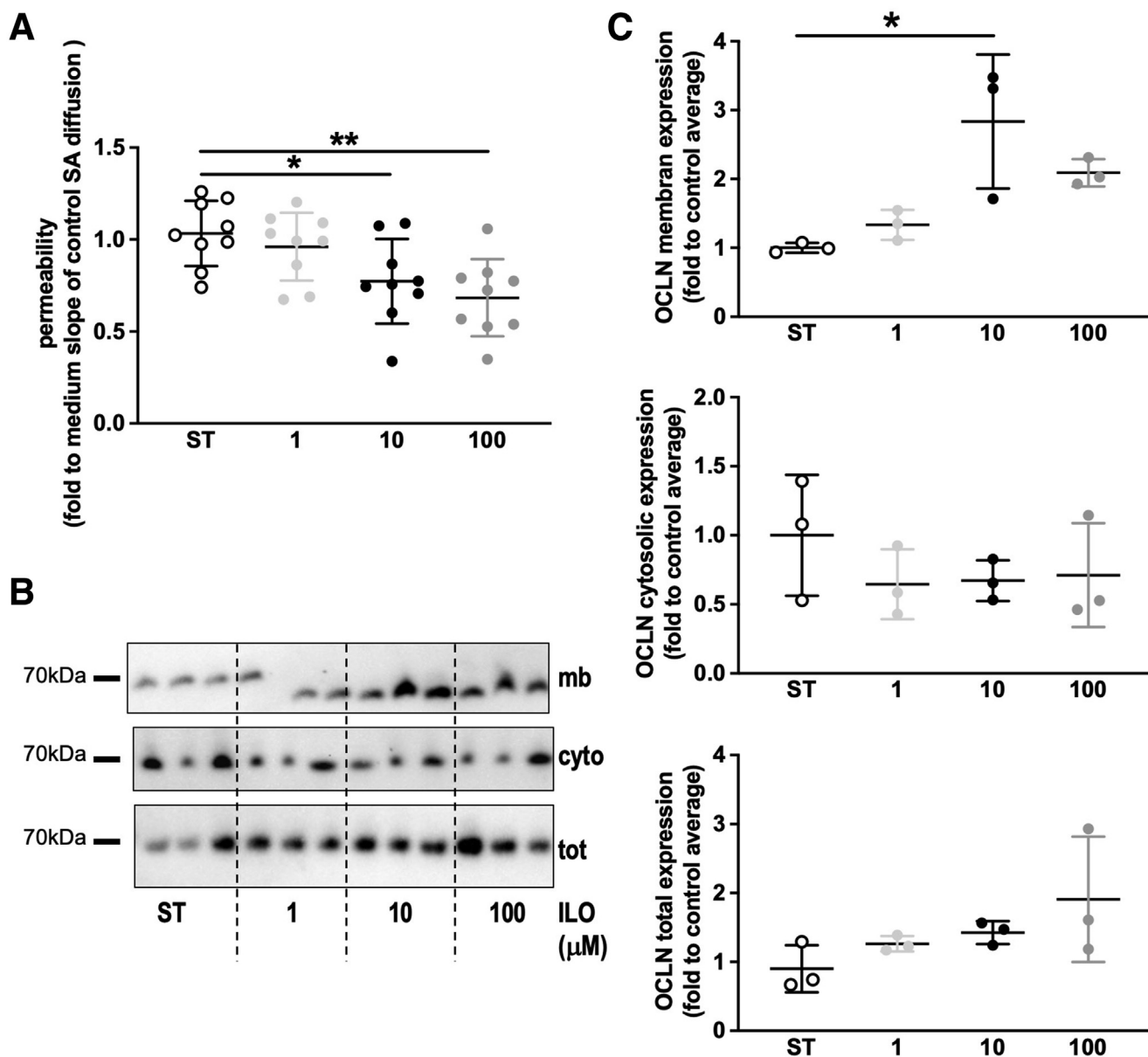
Figure 9. Dose response of PGI$_2$ analog iloprost on mice colon explant permeability and occludin membrane location. (*A–C*) Potential of PGI$_2$ to regulate occludin and reduce IEB permeability induced by apoptosis was assessed on mouse colon explants treated for 16 hours with staurosporine (ST, 1 μmol/L), without or with 4-hour pretreatment with 1, 10, or 100 μmol/L iloprost (ILO). Paracellular permeability measured in Ussing chambers by sulfonic acid flux through mouse tissues after the mentioned treatments (*A*). Occludin membrane (mb), cytosolic (cyto), and total (tot) expression were assessed by Western blot after cell fractionation (*B*) and quantified (*C*). Data represent means ± SEM of 3–9 explants per group. Nonparametric Mann-Whitney test, **$P < .005$ or *$P < .05$.

surgical resections came from patients with severe forms of IBD, biopsies came from patients with light to moderate clinical forms of IBD (Mayo UC-DAI from 0 to 8; Harvey-Bradshaw Index from 0 to 7). The location of the samples and main clinical features of patients are mentioned in Tables 1–4.

Biopsy Supernatants

On removal, biopsies were rapidly weighed and immersed in hard plastic tubes containing 1 mL Hank's buffered saline solution per 10 mg biopsy sample and continuously oxygenated (95% O$_2$/5% CO$_2$) at 37°C. After a 20-minute incubation, the solution was removed and centrifuged at 200g for 10 minutes before being filtered with centrifuge tube filters (0.22 μm, SPIN-X) to remove bacterial components. Supernatant aliquots (200 μL) were stored at –80°C until assayed.

PUFA Metabolite Profiling

n-6/*n*-3 PUFA-derived metabolite dosages were performed as described by Le Faouder et al[87] from biopsy supernatants.

Data Preprocessing and Analysis

Data preprocessing was performed using the Metaboanalyst web interface (www.metaboanalyst.ca).[88] Briefly, preprocessing of the data matrix (concentrations) was performed by removing missing values. The data matrix was transformed using a generalized logarithm and scaled using autoscaling method (mean-centering and division by the standard deviation of each variable). Heatmap and
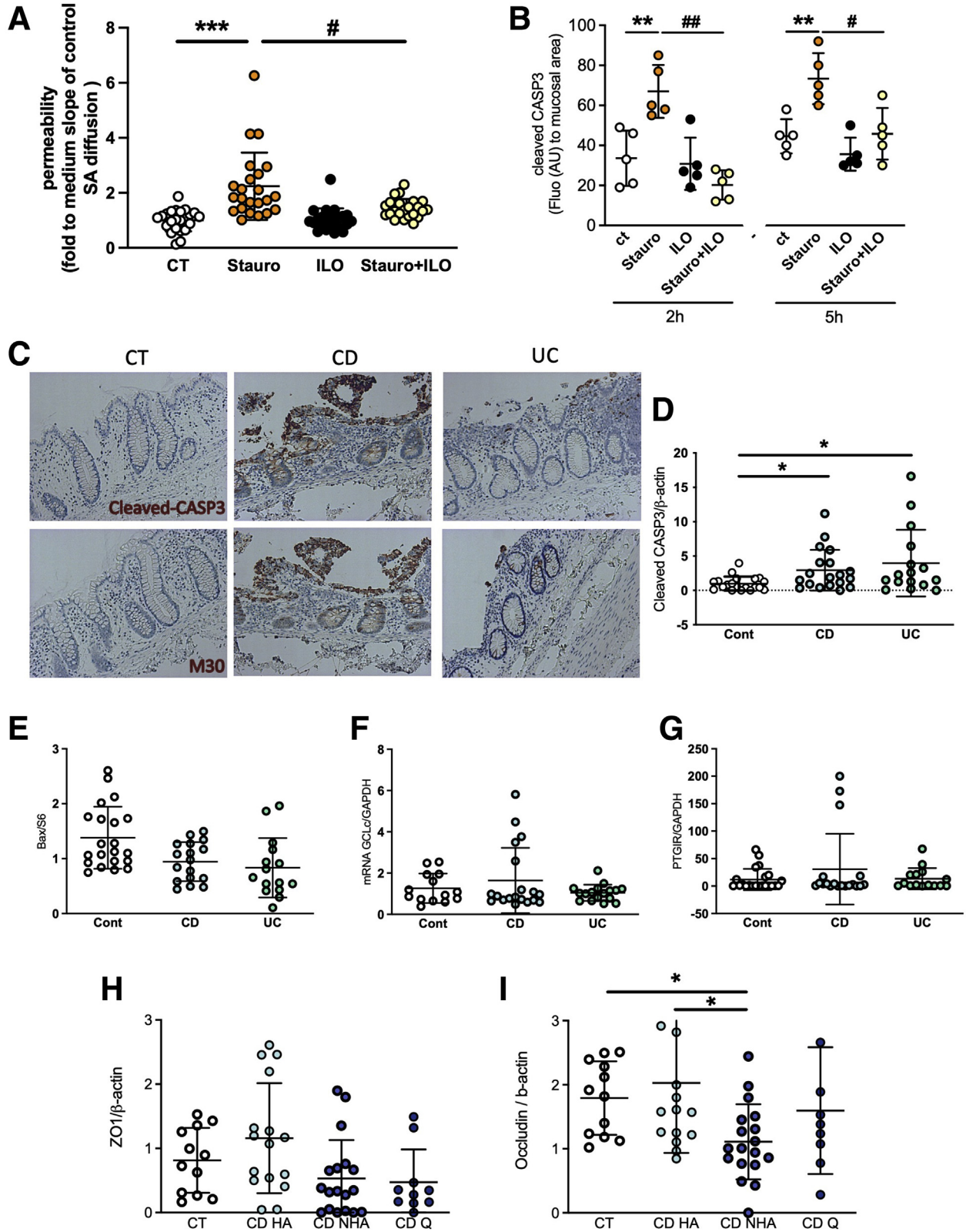
hierarchical clustering presenting group averages and metabolite z-scores was performed on both samples and features using a Pearson distance measure and average clustering. The heatmap and correlation of metabolites were done using a Spearman rank correlation distance measure. The pattern hunter was performed on 6-ketoPGF$_{1\alpha}$ with a Pearson distance measure. One-way analysis of variance (ANOVA) was calculated with an adjusted P value cutoff of .05 and a Fisher least significant difference post hoc test.

Human Explants

Human explants were obtained from human colon samples (Table 2) washed with cold Krebs's solution and from which the muscle layers and submucosa were removed. Mucosa explants (30–40 mg) were maintained in culture in RPMI/Ham's F12 medium (v/v) supplemented with 0.01% bovine serum albumin, 100 IU/mL penicillin, and 100 μg/mL streptomycin and fungizone (1%) at 37°C with 95% O_2 and 5% CO_2 under gentle agitation. Explants were incubated with 10 μmol/L iloprost 4 hours before addition of 1 μmol/L staurosporine. After 18 hours in culture, explants were placed in Ussing chambers for permeability measurement.

Mucosa Histology and Molecular Analyses

Human surgical resections (Table 3) were washed with cold Krebs's solution, and then the mucosa was removed and fixed for 1 hour in 4% paraformaldehyde solution or snap frozen for further analysis (immunostaining or real-time quantitative polymerase chain reaction [qPCR]).

Biopsy Permeability

On removal, biopsies were placed in Ussing chambers and incubated with 10 μmol/L iloprost 1 hour before permeability measurement.

Caco-2 Culture, TEER, and Permeability Measurement In Vitro

The human IEC line Caco-2 was obtained from American Type Culture Collection (Manassas, VA) and cultured in Dulbecco modified Eagle medium containing 4.5 g/L glucose (Gibco, Life Technologies, Carlsbad, CA) supplemented with 10% heat-inactivated fetal calf serum, 2 mmol/L glutamine, 100 IU/mL penicillin, and 100 μg/mL streptomycin. For TEER and permeability experiments, 100,000 Caco-2 cells were seeded onto 24-well Transwell filters coated with collagen I. The metabolite 6-ketoPGF$_{1\alpha}$ (10 μmol/L; Cayman Chemical Co, Ann Arbor, MI) or 10 μmol/L iloprost (Cayman Chemical Co), 100 ng/mL epoprostenol (GlaxoSmithKline, Brentford, UK, or Panpharma, Luitre-Dompierre, France), or solvent was added the following day in the basolateral compartment. To determine the effect of 6-ketoPGF$_{1\alpha}$ or iloprost on IEB resistance, the TEER was measured 1 day after treatment with an epithelial voltohmmeter (EVOM; World Precision Instruments, Inc, Sarasota, FL). To determine the effect of these same drugs on IEB permeability, 50 μL of the apical medium was replaced by 50 μL fluorescein–5.6 sulfonic acid (1 mg/mL; Invitrogen, Carlsbad, CA). The fluorescence level of basolateral aliquots (150 μL) was measured every 30 minutes for a period of 180 minutes using a fluorimeter (Varioskan; Thermo SA, France). Paracellular permeability was determined by averaging the slope change in fluorescence intensity over time by linear regression fit model.

DSS-Induced Colitis and In Vivo Permeability Assessment

Colitis was induced in 8-week-old male C57BL/6NRJ mice (Janvier Labs, Le Genest-Saint-Isle, France) by adding 4% (w/v) DSS (MP Biomedicals, Santa Ana, CA) to the drinking water, which was renewed every day for 4 days. For in vivo assessment of PGI$_2$ effect, epoprostenol (1 μg/mL in phosphate-buffered saline [PBS]) or vehicle (PBS; given in 3 intraperitoneal injections of 100 μL at the beginning, middle, and end of the light cycle) (Figure 3A). Four mice per cage were subjected to a 12-hour light/12-hour dark cycle with free access to food (Safe, Augy, France) and water. Animals were weighed daily; on the last day, animals received 120 μL of a solution containing 300 mg red carmine, 50 mg fluorescein–5.6 sulfonic acid, 50 mg horseradish peroxidase (HRP) (Sigma-Aldrich, St Louis, MO), and 5 mL 0.5% carboxymethylcellulose by

Figure 10. (See previous page). **PGI$_2$ analog iloprost prevents human IEB breakdown ex vivo, and mucosa from IBD patients present increased apoptosis and reduced occludin expression.** (A and B) Potential of PGI$_2$ to block IEB breakdown induced by apoptosis was assessed on human colon explants treated without (CT) with staurosporine (Stauro, 1μmol/L) for 20 hours (A) and the indicated time (B), without or with 4-hour 10 μmol/L iloprost pretreatment (ILO). Paracellular permeability measured in Ussing chambers by sulfonic acid flux through human mucosal colonic samples from control patients after the mentioned treatment (A). Data represent means ± SEM of 6 explants per condition and per patient with 4 different patients. Quantification of cleaved caspase-3 staining relative to mucosal area was quantified in 5 explants per group (B). Two-way ANOVA followed by Bonferroni post hoc tests. ***$P < .001$ (for Stauro factor effects), **$P < .05$ (for Stauro factor effects), or #$P < .05$ (for ILO factor effects). (C–F) Epithelial apoptosis was evaluated in mucosa from control (CT), CD, or UC patients by Western blot analysis, immunostaining, or qPCR. Representative immunostaining of cleaved caspase-3 or cytodeath M30 from CT, CD, and UC patients (C; scale bar: 200 μm). Quantification of cleaved caspase-3 normalized to β-actin expression observed by Western blot (D). Measurement of *BAX* (E), *BCL2* (F), and *PTGIR* (G) mRNA. Data represent means ± SEM of mucosa lysates from CT (n = 20), CD (n = 20), and UC (n = 16) patients. Nonparametric Mann-Whitney test, *$P < .05$. (G and H) Quantification of ZO-1 (H) and occludin (I) expression normalized to β-actin expression observed by Western blot of biopsies from control, quiescent CD, and active CD HA and UHA. Data represent means ± SEM of mucosa lysates from CT (n = 12), active CD (n = 16), and quiescent CD (n = 9) patients. Nonparametric Mann-Whitney test, *$P < .05$.
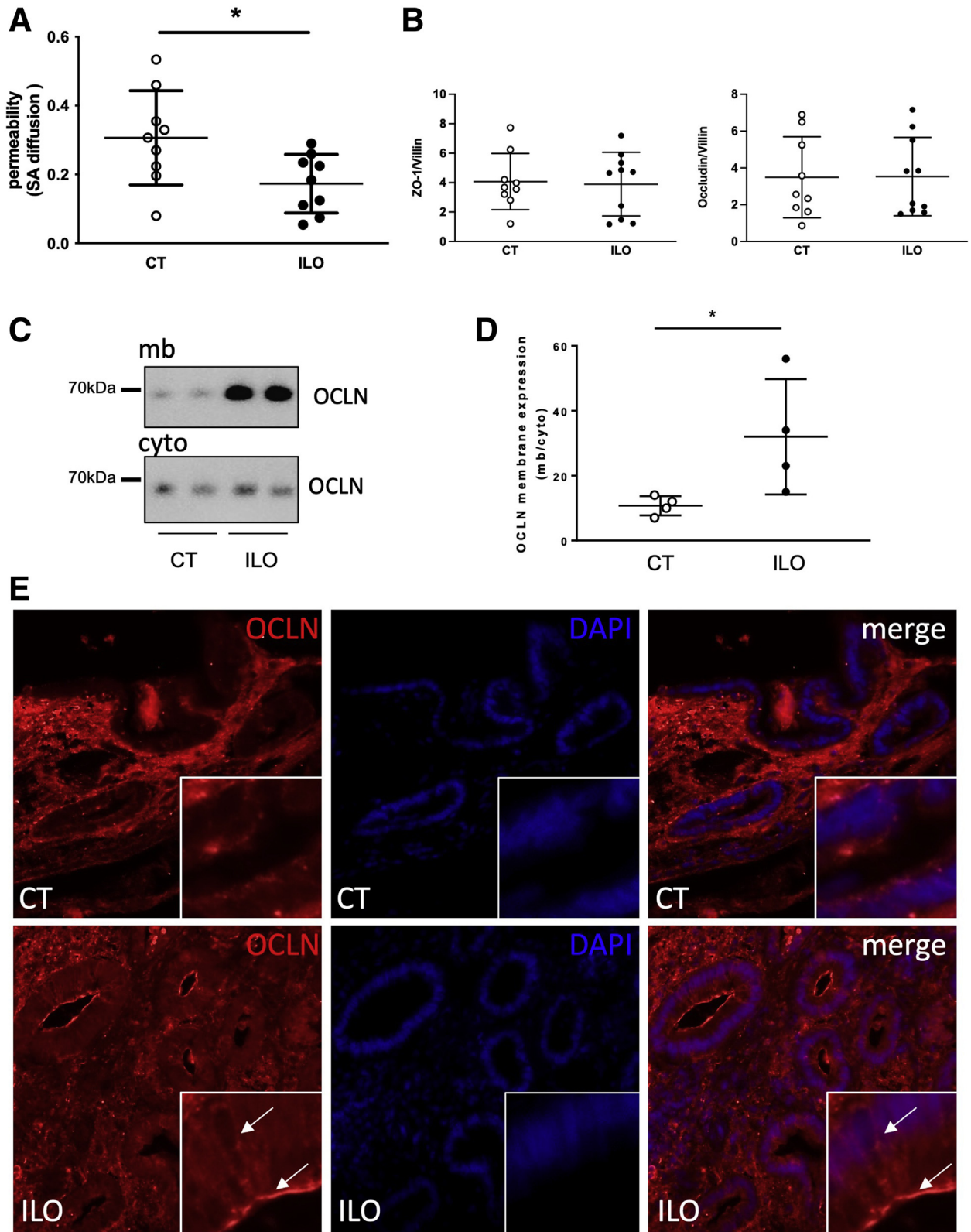
Figure 11. PGI$_2$ analog iloprost reduces permeability and induces occludin membrane location of biopsies from IBD patients. (*A*) Paracellular permeability of biopsies from IBD patients measured by sulfonic acid (SA) flux in Ussing chambers after 1-hour pretreatment with 10 μmol/L iloprost (PGI$_2$) or without (CT). IBD patient (n = 9) data represent the mean SA flux of 2 biopsies per condition per patient. *$P < .05$ paired *t* test. (*B*) Quantification of ZO-1 and occludin expression normalized to villin expression observed by Western blot of biopsies from IBD patients with or without ILO treatment. (*C*) Occludin membrane (mb) and cytosolic (cyto) expressions were assessed by Western blot after cell fractionation (*C*) and quantified (*D*). Data represent means ± SEM of 4 pools of 2 biopsies per group. Nonparametric Mann-Whitney test, *$P < .05$. (*E*) Representative occludin (OCLN) or DAPI staining of human biopsies with or without ILO treatment (scale bar: 50 μm).

Table 1. Main Clinical Features of Patients Used for Biopsy Supernatant Analyses

Patient (n)	Explant location (n)	Age at surgery, y (minimum–maximum)	Sex (M/F)	Treatment received the month before surgery (n)
Control (16)	Colon (16)	45.9 (29–73)	6/10	None (16)
CD (27)	Colon (27)	36.3 (20–48)	16/11	None (2) Anti-TNF (7) Anti-TNF + others[a] (8) Others[a] (10)
UC (19)	Colon (19)	40.6 (21–57)	12/7	None (2) Anti-TNF (3) Anti-TNF + others[a] (3) Others[a] (11)

CD, Crohn's disease; TNF, tumor necrosis factor; UC, ulcerative colitis.
[a]Immunosuppressors and/or anti-inflammatory.

gavage and were placed in individual cages. The DAI was calculated on the basis of stool consistency observed during the 4 hours after gavage (0 = hard stool, 1 = soft or liquid stool) and gross bleeding (0 = no blood, 1 = blood) and was composed of scores from 0 to 2. After 4 hours, blood was collected from the tail vein, and paracellular permeability was evaluated by collecting 5 μL of plasma. The fluorescence of each sample was measured using an automatic microplate reader (Varioskan; Thermo Fisher Scientific, Carlsbad, CA). Transepithelial permeability to HRP was measured by an enzymatic activity assay with 3,3',5,5'-tetramethylbenzidine reagent (BD Bioscience, San Jose, CA). Mice were euthanized, and colon fragments were collected and fixed 1 hour in 4% paraformaldehyde in PBS or snap frozen for further analyses (immunostaining or qPCR). All experiments were approved by the Ethics Committee for Animal Experimentation of Pays de la Loire (study no. 01953.01).

qPCR Analysis

Mucosal fragments from control and IBD patients or colon samples from mice were lysed in RA1 buffer (Macherey-Nagel, Hoerdt, France), and total RNA was extracted with a Nucleospin RNAII kit according to the manufacturer's recommendations (Macherey-Nagel). Purified mRNA (1 μg) was denatured and processed for reverse transcription using Superscript III reverse transcriptase (Invitrogen). PCR amplifications were performed using the Absolute Blue SYBR green fluorescein kit (Roche, Carlsbad, CA) or the Taqman Gene Expression Assay (Life

Technologies) and run on a StepOnePlus system (Life Technologies). The following primers from Life Technologies were used for Taqman assays: IL22 (Mm01226722_g1), IL17a (Mm00439618_m1), IL4 (Mm00445259_m1), IFN-γ (Mm01168134_m1), and ribosomal protein S6 (Mm02342456_g1). Sequences of primers (Sigma-Aldrich) used for SYBR green assays are mentioned in Table 5.

Preparation of Cytosolic and Total Membrane Fractions

Membrane and cytosolic fractions were obtained as previously described.[89] Briefly, mouse explants or biopsies were harvested in 400 μL of buffer A (10 mmol/L HEPES, pH 7.9, 1.5 mmol/L MgCl$_2$, 10 mmol/L KCl, 0.5 mmol/L dithiothreitol), and after 10 strokes in a syringe with a G25 needle, homogenates were centrifuged for 10 minutes at 2000 rpm. A 0.11 volume of buffer B (0.3 mol/L HEPES, pH 7.9, 0.3 mol/L MgCl$_2$, 1.4 mol/L KCl) was then added to the carefully decanted supernatants and centrifuged for 60 minutes at 100,000g. The high-speed pellet represents the "membrane fraction," and the high-speed supernatant represents the "cytosolic fraction." The membrane fractions were washed twice and resuspended in 1× Laemli buffer. Then Laemli was added to the cytosolic fractions, and all fractions were denatured at 95°C for 10 minutes and then put on ice before Western blotting analysis.

Western Blotting

Mucosal fragments from control and IBD patients or colon samples from mice were lysed in RA1 buffer

Table 2. Main Clinical Features of Patients Used for Explants

Patient (n)	Explant location (n)	Age at surgery, y (minimum–maximum)	Sex (M/F)	Treatment at time of surgery (n)
Control, cancer at a distance from tumor (2), other (2)	Colon (4)	63 (48–83)	2/2	None (3) Immunosuppressors (1)

Table 3. Main Clinical Features of Patients Used for Mucosa Molecular Analyses

Patient (n)	Explant location (n)	Age at surgery, y (minimum–maximum)	Sex (M/F)	Treatment at time of surgery (n)
Control, cancer at a distance from tumor (20)	Ileum (4) Colon (15) Rectum (1)	61.8 (38–82)	14/6	None (19) Radiotherapy (1)
CD (20)	Ileum (8) Colon (12) Rectum (0)	37.4 (17–63)	9/11	None (7) Mesalamine (1) IS (4) MTT + IS (1) Anti-TNF (6) Anti-TNF+IS (1)
UC (16)	Ileum (2) Colon (11) Rectum (3)	43 (19–60)	8/8	None (11) Mesalamine (1) IS (0) MTT + IS (0) Anti-TNF (4) Anti-TNF+IS (0)

CD, Crohn's disease; IS, immunosuppressors; MTT, methotrexate; TNF, tumor necrosis factor; UC, ulcerative colitis.

(Macherey-Nagel), and total protein extraction was performed with a Nucleospin RNAII kit according to the manufacturer's recommendations. For Caco-2 filters, cells were washed with ice-cold PBS and lysed in ice-cold RIPA buffer complete with protease inhibitor (Roche) and serine-threonine phosphatase inhibitor (Sigma-Aldrich) cocktails. Nuclei and intact cells were removed by centrifugation at 10,000g for 10 minutes at 4°C. Samples were processed for electrophoresis using an MES Sodium Dodecyl Sulfate buffer kit (Invitrogen). Samples were separated on 4%–12% Bis-Tris or 3%–8% Tris-Acetate gels (Life Technologies). Proteins were transferred to nitrocellulose membranes with the iBlot system (Life Technologies). After blocking with Tris-buffered saline/0.1% Tween-20/5% nonfat dry milk for 30 minutes, blots were incubated overnight at 4°C with the following primary antibodies diluted in Tris-buffered saline/5% nonfat dry milk: mouse anti-ZO-1 (1:200; Thermo Fisher Scientific), rabbit anti-occludin (1:500; Abcam, Cambridge, UK), rabbit anti-junctional adhesion molecule-A (1:500; Bethyl Laboratories, Montgomery, TX), rabbit anti-claudin-2 (1:200; Life Technologies), rabbit anti-cingulin (1:500; Santa Cruz Biotechnology, Dallas, TX), mouse anti-phospho-MLC20 (1:200; Cell Signaling Technology, Danvers, MA), rabbit anti-PCNA (1:500; Abcam), rabbit anti-phospho-Akt and anti-Akt (1:400; Cell Signaling Technology), rabbit anti-cleaved caspase-3 (1:200; Cell Signaling Technology), and mouse anti-β-actin (1:10,000; Sigma-Aldrich). Immunoblots were probed with the appropriate HRP-conjugated secondary antibodies (Life Technologies) and visualized by chemiluminescence (Bio-Rad, Hercules, CA) using a Gel-Doc imager and Image Lab Software (Bio-Rad). The value of protein immunoreactivity was normalized to β-actin immunoreactivity and expressed as the fold-increase relative to the average of control values taken as 1.

Immunohistochemistry and Histopathology

Formalin-fixed human and mice tissues were embedded in paraffin using an embedding station (LEICA EG1150C, Wetzlar, Germany) and cut into 3-μm sections using a microtome (LEICA RM2255).

Table 4. Main Clinical Features of Patients Used for Biopsy Permeability Analyses

Patient (n)	Explant localization (n)	Age at surgery, y (minimum–maximum)	Sex (M/F)	Treatment at time of surgery (n)
CD (7), UC (2)	Ileum (4) Colon (14) Rectum (0)	32.7 (17–63)	5/4	None (0) Mesalamine (1) IS (1) MTT+IS (1) Anti-TNF (3) Anti-TNF+IS (3)

CD, Crohn's disease; IS, immunosuppressors; MTT, methotrexate; TNF, tumor necrosis factor; UC, ulcerative colitis.

Table 5. Sequences of Primers Used for SYBR Green Assays

Prostaglandin I2 Receptor (IP, PTGIR) #NM_000960.3
  Forward Primer: 5'-CTCTCACGATCCGCTGCTTC-3'
  Reverse Primer: 5'-GAGCTGGGAAAGGGGTGTCT-3'

Tumor necrosis factor alpha (TNFα) # NM_013693.3
  Forward Primer: 5'-GAACTTCGGGGGTGATCGGTCC-3'
  Reverse Primer: 5'-GCCACTCCAGCTGCTCCTCC-3'

Interleukin 1 beta (IL1β) # NM_008361.4
  Forward Primer : 5'-GCCTCGTGCTGTCGGACCCATA-3'
  Reverse Primer : 5'-TTGAGGCCCAAGGCCACAGGT-3'

Interleukin 6 (IL6) #NM_031168.2
  Forward Primer : 5'-TCCAGTTGCCTTCTTGGGAC-3'
  Reverse Primer : 5'-AGTCTCCTCTCCGGACTTGT-3'

Ribosomal protein S6 (RPS6) # NM_001010.2
  Forward Primer : 5'-CCAAGCTTATTCAGCGTCTTGTTACTCC-3'
  Reverse Primer : 5'-CCCTCGAGTCCTTCATTCTCTTGGC-3'

Fluorescence

Slides were deparaffinized with 2 xylene baths (5 minutes each) and incubated in 4 ethanol baths (100%, 95%, 70%, and 70%, respectively; 3 minutes each). After a rinse in distilled water, slides were washed in PBS, and antigen retrieval was performed using a sodium citrate solution (2.94 g sodium citrate tribasic, 1 L distilled water, 500 μL Tween-20, pH 6) at 95°C for 20 minutes. Slides were incubated in 100 mmol/L NH_4Cl for 15 minutes before incubation in PBS/0.5% Triton X-100 for 1 hour and blocking for 2 hours in 10% horse serum in PBS/0.5% Triton X-100. Primary antibodies for cleaved caspase-3 (1:100; rabbit polyclonal, 9661; Cell Signaling Technology), cytodeath M30 (1:100; Roche), or occludin (1:100; rabbit polyclonal, Abcam) were incubated on slides overnight at 4°C before incubating with the appropriate secondary antibody for 2 hours at room temperature. Images were acquired with an Olympus IX 50 or Zeiss Axio Observer fluorescence microscope coupled to a digital camera (model DP71, Olympus, Tokyo, Japan or Hamamatsu Photonics, Hamamatsu, Japan) and analyzed with Cell B software (Soft Imaging System; Olympus) or Zen software. The fluorescence of the mucosal area was reported to estimate cleaved caspase-3 expression using ImageJ software (National Institutes of Health, Bethesda, MD).

Histologic Score

Hematein Phloxin Safran coloration allowed the visualization of tissue morphology. Tissue damage was scored in a blinded manner by quantifying destruction of mucosal architecture, cellular infiltration, muscle thickening, and loss of goblet cells. The extent of destruction of normal mucosal architecture was scored as 0–3 (0 = no destruction, 1 = 1/3 basal destruction, 2 = 2/3 basal destruction, 3 = loss of crypt and epithelium). The presence and degree of cellular infiltration were also scored as 0–3 when the infiltration was normal, around the crypt basis, reaching the muscularis mucosae, and reaching the submucosa, respectively. The extent of muscle thickening was scored as 0–3 when the thickening was none, mild, moderate, or massive, respectively. The presence or absence of goblet cell depletion was scored as 0 (normal) or 1 (massive depletion). An extension factor of 1–4 was applied when the criteria measured reached 25%, 50%, 75%, or 100% of the fragment analyzed.

Mouse Colonic Explants

Colons from C57BL/6 NRJ mice were removed and washed 3 times in cold Krebs's solution. For immunostaining, colon pieces were incubated with biopsy medium (Dulbecco modified Eagle medium containing 4.5 g/L glucose, 2.5% fetal bovine serum, 100 IU/mL penicillin, 100 μg/mL streptomycin, 20 μg/mL gentamycin, and 1.1 μg/mL AmphoB) containing 10 μmol/L iloprost at 37°C with 95% O_2 and 5% CO_2. After 1 hour, 1 μmol/L staurosporine (Promocell, Heidelberg, Germany) was added to colon segments for 2 hours before fixing tissues for 1 hour in 4% paraformaldehyde in PBS. Apoptosis scores were assessed on these samples by quantifying cells positive for cleaved caspase-3 staining. The extent of apoptosis was scored as 0–2 (0 = no positive cells, 1 = 1/2 positive basal cells, 2 = positivity along the entire crypt). An extended score factor of 1–4 was applied when positivity reached 25%, 50%, 75%, or 100% of the fragment analyzed, respectively. For the paracellular permeability measurement, 8 pieces of each colon were incubated with biopsy medium containing 1–100 μmol/L iloprost (Figure 7) as described earlier. After 4 hours, 1 μmol/L staurosporine was added to colon segments and incubated overnight. Twenty-four hours after the start of the incubation process, colon pieces were mounted in Ussing chambers, and paracellular permeability was measured as detailed above.

Ex Vivo Permeability Assessment in Ussing Chambers

Human biopsies and human or mice explants were mounted in Ussing chambers (0.011 or 0.03 cm^2 exposed surface area, respectively; Physiologic Instruments, San Diego, CA) as previously described.[90] Each chamber contained 2 mL of Ham's/F12 medium (Invitrogen) maintained at 37°C and continuously gassed with 95% O_2 and 5% CO_2. After 30 minutes of equilibration, 200 μL of apical medium was replaced by 200 μL of fluorescein–5.6 sulfonic acid (1 mg/mL). The fluorescence level of basolateral aliquots (150 μL) was measured every 30 minutes for a period of 180 minutes to evaluate paracellular permeability using a Varioskan automatic microplate reader. Samples were then used for preparation of cytosolic and total membrane fractions and further Western blotting analysis.

Drugs

Iloprost and epoprostenol have different selectivity for prostanoid receptors. Iloprost can bind to and activate EP1 with greater affinity than IP, and epoprostenol can bind to and activate EP3 receptors with 20 times less affinity than IP.[80] The methyl acetate in which iloprost was supplied was evaporated under a gentle stream of nitrogen and immediately resuspended in dimethyl sulfoxide to

obtain a 10 or 100 mmol/L stock solution. The same dilution of dimethyl sulfoxide alone was always used in control wells.

Statistics

Except for PUFA-metabolite profiling, all graphics were drawn and analyzed using GraphPad Prism 5.0 Software (GraphPad Software, La Jolla, CA). Values are expressed as means ± standard error of the mean (SEM). The significance of differences was determined using either 2-way ANOVA followed by Bonferroni post hoc test or nonparametric Mann-Whitney test using GraphPad Prism 5.0. Statistical significance was reached when $P <.05$. For PUFA-metabolite profiling, 1-way ANOVA was performed using www.metaboanalyst.ca with an adjusted P value cutoff of .05 and a Fisher least significant difference post hoc test.

References

1. Molodecky NA, Soon IS, Rabi DM, Ghali WA, Ferris M, Chernoff G, Benchimol EI, Panaccione R, Ghosh S, Barkema HW, Kaplan GG. Increasing incidence and prevalence of the inflammatory bowel diseases with time, based on systematic review. Gastroenterology 2012;142:46–54 e42, quiz e30.
2. Ananthakrishnan AN. Epidemiology and risk factors for IBD. Nature Reviews Gastroenterology Hepatology 2015; 12:205–217.
3. Gu YB, Zhong J. Endoscopic management of stricturing Crohn's disease. J Dig Dis 2020;21:351–354.
4. Spinelli A, Armuzzi A, Ciccocioppo R, Danese S, Gionchetti P, Luglio G, Orlando A, Rispo A, Rizzello F, Sofo L, Solina G, Poggioli G. Management of patients with complex perianal fistulas in Crohn's disease: optimal patient flow in the Italian clinical reality. Dig Liver Dis 2020;52:506–515.
5. Xavier RJ, Podolsky DK. Unravelling the pathogenesis of inflammatory bowel disease. Nature 2007;448:427–434.
6. Khor B, Gardet A, Xavier RJ. Genetics and pathogenesis of inflammatory bowel disease. Nature 2011; 474:307–317.
7. Arrieta MC, Bistritz L, Meddings JB. Alterations in intestinal permeability. Gut 2006;55:1512–1520.
8. Okamoto R, Watanabe M. Cellular and molecular mechanisms of the epithelial repair in IBD. Dig Dis Sci 2005;50(Suppl 1):S34–S38.
9. Arrieta MC, Madsen K, Doyle J, Meddings J. Reducing small intestinal permeability attenuates colitis in the Il10 gene-deficient mouse. Gut 2009;58:41–48.
10. Irvine EJ, Marshall JK. Increased intestinal permeability precedes the onset of Crohn's disease in a subject with familial risk. Gastroenterology 2000;119:1740–1744.
11. Arnott ID, Kingstone K, Ghosh S. Abnormal intestinal permeability predicts relapse in inactive Crohn disease. Scand J Gastroenterol 2000;35:1163–1169.
12. Wyatt J, Vogelsang H, Hubl W, Waldhoer T, Lochs H. Intestinal permeability and the prediction of relapse in Crohn's disease. Lancet 1993;341:1437–1439.
13. Soderholm JD, Peterson KH, Olaison G, Franzen LE, Westrom B, Magnusson KE, Sjodahl R. Epithelial permeability to proteins in the noninflamed ileum of Crohn's disease? Gastroenterology 1999;117:65–72.
14. Baert F, Moortgat L, Van Assche G, Caenepeel P, Vergauwe P, De Vos M, Stokkers P, Hommes D, Rutgeerts P, Vermeire S, D'Haens G. Mucosal healing predicts sustained clinical remission in patients with early-stage Crohn's disease. Gastroenterology 2010; 138:463–468, quiz e410–e461.
15. Okamoto R, Watanabe M. Role of epithelial cells in the pathogenesis and treatment of inflammatory bowel disease. J Gastroenterol 2016;51:11–21.
16. Sharon P, Ligumsky M, Rachmilewitz D, Zor U. Role of prostaglandins in ulcerative colitis: enhanced production during active disease and inhibition by sulfasalazine. Gastroenterology 1978;75:638–640.
17. Shannon VR, Stenson WF, Holtzman MJ. Induction of epithelial arachidonate 12-lipoxygenase at active sites of inflammatory bowel disease. Am J Physiol 1993; 264:G104–G111.
18. Ikehata A, Hiwatashi N, Kinouchi Y, Yamazaki H, Ito K, Toyota T. Altered leukotriene B4 metabolism in colonic mucosa with inflammatory bowel disease. Scand J Gastroenterol 1995;30:44–49.
19. Ligumsky M, Karmeli F, Sharon P, Zor U, Cohen F, Rachmilewitz D. Enhanced thromboxane a2 and prostacyclin production by cultured rectal mucosa in ulcerative colitis and its inhibition by steroids and sulfasalazine. Gastroenterology 1981;81:444–449.
20. Lauritsen K, Staerk Laursen L, Bukhave K, Rask-Madsen J. Longterm olsalazine treatment: pharmacokinetics, tolerance and effects on local eicosanoid formation in ulcerative colitis and Crohn's colitis. Gut 1988; 29:974–982.
21. Le Loupp AG, Bach-Ngohou K, Bourreille A, Boudin H, Rolli-Derkinderen M, Denis MG, Neunlist M, Masson D. Activation of the prostaglandin D2 metabolic pathway in Crohn's disease: involvement of the enteric nervous system. BMC Gastroenterology 2015;15:112.
22. Hawkey CJ, Karmeli F, Rachmilewitz D. Imbalance of prostacyclin and thromboxane synthesis in Crohn's disease. Gut 1983;24:881–885.
23. Zifroni A, Treves AJ, Sachar DB, Rachmilewitz D. Prostanoid synthesis by cultured intestinal epithelial and mononuclear cells in inflammatory bowel disease. Gut 1983;24:659–664.
24. Masoodi M, Pearl DS, Eiden M, Shute JK, Brown JF, Calder PC, Trebble TM. Altered colonic mucosal polyunsaturated fatty acid (pufa) derived lipid mediators in ulcerative colitis: new insight into relationship with disease activity and pathophysiology. PloS One 2013;8:e76532.
25. Ajuebor MN, Singh A, Wallace JL. Cyclooxygenase-2-derived prostaglandin D(2) is an early anti-inflammatory signal in experimental colitis. Am J Physiol Gastrointest Liver Physiol 2000;279:G238–G244.
26. Gilroy DW, Colville-Nash PR, McMaster S, Sawatzky DA, Willoughby DA, Lawrence T. Inducible cyclooxygenase-derived 15-deoxy(delta)12-14pgj2 brings about acute inflammatory resolution in rat pleurisy by inducing neutrophil and macrophage apoptosis. Faseb J 2003; 17:2269–2271.

27. Hokari R, Kurihara C, Nagata N, Aritake K, Okada Y, Watanabe C, Komoto S, Nakamura M, Kawaguchi A, Nagao S, Urade Y, Miura S. Increased expression of lipocalin-type-prostaglandin D synthase in ulcerative colitis and exacerbating role in murine colitis. Am J Physiol Gastrointest Liver Physiol 2011;300:G401–G408.

28. Li J, Kong D, Wang Q, Wu W, Tang Y, Bai T, Guo L, Wei L, Zhang Q, Yu Y, Qian Y, Zuo S, Liu G, Liu Q, Wu S, Zang Y, Zhu Q, Jia D, Wang Y, Yao W, Ji Y, Yin H, Nakamura M, Lazarus M, Breyer RM, Wang L, Yu Y. Niacin ameliorates ulcerative colitis via prostaglandin D2-mediated D prostanoid receptor 1 activation. EMBO Molecular Medicine 2017;9:571–588.

29. Rajakariar R, Hilliard M, Lawrence T, Trivedi S, Colville-Nash P, Bellingan G, Fitzgerald D, Yaqoob MM, Gilroy DW. Hematopoietic prostaglandin D2 synthase controls the onset and resolution of acute inflammation through PgD2 and 15-deoxydelta12 14 pgj2. Proc Natl Acad Sci U S A 2007;104:20979–20984.

30. Vong L, Ferraz JG, Panaccione R, Beck PL, Wallace JL. A pro-resolution mediator, prostaglandin D(2), is specifically up-regulated in individuals in long-term remission from ulcerative colitis. Proc Natl Acad Sci U S A 2010; 107:12023–12027.

31. Gobbetti T, Ducheix S, le Faouder P, Perez T, Riols F, Boue J, Bertrand-Michel J, Dubourdeau M, Guillou H, Perretti M, Vergnolle N, Cenac N. Protective effects of n-6 fatty acids-enriched diet on intestinal ischaemia/reperfusion injury involve lipoxin A4 and its receptor. Br J Pharmacol 2015;172:910–923.

32. Das UN. Inflammatory bowel disease as a disorder of an imbalance between pro- and anti-inflammatory molecules and deficiency of resolution bioactive lipids. Lipids in Health and Disease 2016;15:11.

33. Dennis EA, Norris PC. Eicosanoid storm in infection and inflammation. Nature Reviews Immunology 2015; 15:511–523.

34. Pochard C, Coquenlorge S, Jaulin J, Cenac N, Vergnolle N, Meurette G, Freyssinet M, Neunlist M, Rolli-Derkinderen M. Defects in 15-HETE production and control of epithelial permeability by human enteric glial cells from patients with Crohn's disease. Gastroenterology 2016;150:168–180.

35. Coquenlorge S, Van Landeghem L, Jaulin J, Cenac N, Vergnolle N, Duchalais E, Neunlist M, Rolli-Derkinderen M. The arachidonic acid metabolite 11beta-prostaglandinF2alpha controls intestinal epithelial healing: deficiency in patients with Crohn's disease. Scientific Reports 2016;6:25203.

36. Miyoshi H, VanDussen KL, Malvin NP, Ryu SH, Wang Y, Sonnek NM, Lai CW, Stappenbeck TS. Prostaglandin E2 promotes intestinal repair through an adaptive cellular response of the epithelium. EMBO J 2017;36:5–24.

37. Herminghaus A, Eberhardt R, Truse R, Schulz J, Bauer I, Picker O, Vollmer C. Nitroglycerin and iloprost improve mitochondrial function in colon homogenate without altering the barrier integrity of Caco-2 monolayers. Frontiers in Medicine 2018;5:291.

38. Leers MP, Kolgen W, Bjorklund V, Bergman T, Tribbick G, Persson B, Bjorklund P, Ramaekers FC, Bjorklund B, Nap M, Jornvall H, Schutte B. Immunocytochemical detection and mapping of a cytokeratin 18 neo-epitope exposed during early apoptosis. J Pathol 1999;187:567–572.

39. Lee JY, Wasinger VC, Yau YY, Chuang E, Yajnik V, Leong RW. Molecular pathophysiology of epithelial barrier dysfunction in inflammatory bowel diseases. Proteomes 2018;6:17.

40. Ricciotti E, FitzGerald GA. Prostaglandins and inflammation. Arterioscler Thromb Vasc Biol 2011; 31:986–1000.

41. Sinzinger H, Silberbaver K, Seyfried H. Rectal mucosa prostacyclin formation in ulcerative colitis. Lancet 1979; 1:444.

42. Seyfried H, Sinzinger H, Silberbauer K. [prostacyclin (PGI2) activity in the rectal mucosa of patients with ulcerative colitis (author's transl)]. Wien Klin Wochenschr 1980;92:282–284.

43. Tihanyi K, Rozsa I, Banai J, Dobo I, Bajtai A. Tissue concentrations and correlations of prostaglandins in healthy and inflamed human esophageal and jejunal mucosa. J Gastroenterol 1996;31:149–152.

44. Rehal S, von der Weid PY. Experimental ileitis alters prostaglandin biosynthesis in mesenteric lymphatic and blood vessels. Prostaglandins Other Lipid Mediat 2015; 116–117:37–48.

45. Sadler T, Bhasin JM, Xu Y, Barnholz-Sloan J, Chen Y, Ting AH, Stylianou E. Genome-wide analysis of DNA methylation and gene expression defines molecular characteristics of Crohn's disease-associated fibrosis. Clinical Epigenetics 2016;8:30.

46. Whittle BJ. Inhibition of prostacyclin (PGI2) formation in the rat small-intestine and gastric mucosa by the ulcerogen, indomethacin [proceedings]. Br J Pharmacol 1978; 64:438P.

47. Robert A. Experimental production of duodenal ulcers. Biol Gastroenterol (Paris) 1974;7:145–161.

48. Sharon P, Cohen F, Zifroni A, Karmeli F, Ligumsky M, Rachmilewitz D. Prostanoid synthesis by cultured gastric and duodenal mucosa: possible role in the pathogenesis of duodenal ulcer. Scand J Gastroenterol 1983;18:1045–1049.

49. Hillier K, Smith CL, Jewell R, Arthur MJ, Ross G. Duodenal mucosa synthesis of prostaglandins in duodenal ulcer disease. Gut 1985;26:237–240.

50. Robert A, Schultz JR, Nezamis JE, Lancaster C. Gastric antisecretory and antiulcer properties of PGE2, 15-methyl PGE2, and 16, 16-dimethyl PGE2: intravenous, oral and intrajejunal administration. Gastroenterology 1976;70:359–370.

51. Cohen MM. Mucosal cytoprotection by prostaglandin E2. Lancet 1978;2:1253–1254.

52. Peng X, Li J, Tan S, Xu M, Tao J, Jiang J, Liu H, Wu B. Cox-1/PGE2/EP4 alleviates mucosal injury by upregulating beta-arr1-mediated Akt signaling in colitis. Scientific Reports 2017;7:1055.

53. Stenson WF. Prostaglandins and epithelial response to injury. Current Opinion in Gastroenterology 2007; 23:107–110.

54. Bach-Ngohou K, Mahe MM, Aubert P, Abdo H, Boni S, Bourreille A, Denis MG, Lardeux B, Neunlist M,

Masson D. Enteric glia modulate epithelial cell proliferation and differentiation through 15-deoxy-12,14-prostaglandin J2. J Physiol 2010;588:2533–2544.

55. Ruwart MJ, Rush BD. Prostacyclin inhibits gastric emptying and small-intestinal transit in rats and dogs. Gastroenterology 1984;87:392–395.

56. Bennett A, Sanger GJ. Prostacyclin relaxes the longitudinal muscle of human isolated stomach and antagonizes contractions to some prostanoids [proceedings]. J Physiol 1980;298:45P–46P.

57. Sanger GJ, Bennett A. Regional differences in the responses to prostanoids of circular muscle from guinea-pig isolated intestine. J Pharm Pharmacol 1980;32:705–708.

58. Thor P, Konturek JW, Konturek SJ, Anderson JH. Role of prostaglandins in control of intestinal motility. Am J Physiol 1985;248:G353–G359.

59. Vermue NA, Den Hertog A, Zaagsma J. Desensitization of PGE2 and PGI2 induced contractions in different smooth muscles of guinea-pig unmasking relaxing properties of prostanoids. Eur J Pharmacol 1987;144:399–403.

60. Paustian PW, Chapnick BM, Feigen LP, Hyman AL, Kadowitz PJ. Effects of 13, 14-dehydroprostacyclin methyl ester on the feline intestinal vascular bed. Prostaglandins 1977;14:1141–1152.

61. Crane BH, Maish TL, Maddox YT, Corey EJ, Szekely I, Ramwell PW. Effect of prostaglandin I2 and analogs on platelet aggregation and smooth muscle contraction. J Pharmacol Exp Ther 1978;206:132–138.

62. Ogawa H, Rafiee P, Fisher PJ, Johnson NA, Otterson MF, Binion DG. Sodium butyrate inhibits angiogenesis of human intestinal microvascular endothelial cells through Cox-2 inhibition. FEBS Lett 2003;554:88–94.

63. Raptis D, Pramateftakis MG, Kanellos I. Our 20-year experience with experimental colonic anastomotic healing. Journal of Medicine and Life 2018;11:5–14.

64. Bostanoglu S, Dincer S, Keskin A, Bostanoglu A, Dursun A, Serim C. Beneficial effect of iloprost on impaired colonic anastomotic healing induced by intraperitoneal 5-fluorouracil infusion. Dis Colon Rectum 1998;41:642–648.

65. Sakaguchi T, Nakamura S, Suzuki S, Baba S, Nakashima M. Endogenous endotoxemia after massive hepatectomy and portal vein stenosis: beneficial effect of a prostaglandin I2 analogue on intestinal permeability. Eur Surg Res 1996;28:341–350.

66. Konturek SJ, Brzozowski T, Radecki T, Pastucki I. Comparison of gastric and intestinal antisecretory and protective effects of prostacyclin and its stable thiaimino-analogue (hoe 892) in conscious rats. Prostaglandins 1984;28:443–453.

67. Dembinski A, Konturek SJ. Effects of E, F, and I series prostaglandins and analogues on growth of gastroduodenal mucosa and pancreas. Am J Physiol 1985;248:G170–G175.

68. Blikslager AT, Roberts MC, Argenzio RA. Prostaglandin-induced recovery of barrier function in porcine ileum is triggered by chloride secretion. Am J Physiol 1999;276:G28–G36.

69. Blume ED, Taylor CT, Lennon PF, Stahl GL, Colgan SP. Activated endothelial cells elicit paracrine induction of epithelial chloride secretion: 6-keto-PGF1alpha is an epithelial secretagogue. J Clin Invest 1998;102:1161–1172.

70. Moriarty KJ, O'Grady J, Rolston DD, Kelly MJ, Clark ML. Effect of prostacyclin (PGI2) on water and solute transport in the human jejunum. Gut 1986;27:158–163.

71. Goerg KJ, Wanitschke R, Becker U, Meyer zum Buschenfelde KH. Effect of the stable prostacyclin analogue iloprost on water and electrolyte transfer of the rat ileum and colon in vivo. Eur J Clin Invest 1988;18:124–127.

72. Qiao L, Kozoni V, Tsioulias GJ, Koutsos MI, Hanif R, Shiff SJ, Rigas B. Selected eicosanoids increase the proliferation rate of human colon carcinoma cell lines and mouse colonocytes in vivo. Biochim Biophys Acta 1995;1258:215–223.

73. Cutler NS, Graves-Deal R, LaFleur BJ, Gao Z, Boman BM, Whitehead RH, Terry E, Morrow JD, Coffey RJ. Stromal production of prostacyclin confers an antiapoptotic effect to colonic epithelial cells. Cancer Res 2003;63:1748–1751.

74. Zushi S, Shinomura Y, Kiyohara T, Minami T, Sugimachi M, Higashimoto Y, Kanayama S, Matsuzawa Y. Role of prostaglandins in intestinal epithelial restitution stimulated by growth factors. Am J Physiol 1996;270:G757–G762.

75. Blikslager AT, Zimmel DN, Young KM, Campbell NB, Little D, Argenzio RA. Recovery of ischaemic injured porcine ileum: evidence for a contributory role of Cox-1 and Cox-2. Gut 2002;50:615–623.

76. Campbell NB, Blikslager AT. The role of cyclooxygenase inhibitors in repair of ischaemic-injured jejunal mucosa in the horse. Equine Vet J Suppl 2000:59–64.

77. Tan XD, Chen YH, Liu QP, Gonzalez-Crussi F, Liu XL. Prostanoids mediate the protective effect of trefoil factor 3 in oxidant-induced intestinal epithelial cell injury: role of cyclooxygenase-2. J Cell Sci 2000;113(Pt 12):2149–2155.

78. Little D, Dean RA, Young KM, McKane SA, Martin LD, Jones SL, Blikslager AT. PI3K signaling is required for prostaglandin-induced mucosal recovery in ischemia-injured porcine ileum. Am J Physiol Gastrointest Liver Physiol 2003;284:G46–G56.

79. Moreno JJ. Eicosanoid receptors: targets for the treatment of disrupted intestinal epithelial homeostasis. Eur J Pharmacol 2017;796:7–19.

80. Clapp LH, Gurung R. The mechanistic basis of prostacyclin and its stable analogues in pulmonary arterial hypertension: role of membrane versus nuclear receptors. Prostaglandins Other Lipid Mediat 2015;120:56–71.

81. Turner JR. Intestinal mucosal barrier function in health and disease. Nature Reviews Immunology 2009;9:799–809.

82. Gitter AH, Wullstein F, Fromm M, Schulzke JD. Epithelial barrier defects in ulcerative colitis: characterization and quantification by electrophysiological imaging. Gastroenterology 2001;121:1320–1328.

83. Yu LC, Flynn AN, Turner JR, Buret AG. Sglt-1-mediated glucose uptake protects intestinal epithelial cells against LPS-induced apoptosis and barrier defects: a novel cellular rescue mechanism? Faseb J 2005;19:1822–1835.

84. Su L, Nalle SC, Shen L, Turner ES, Singh G, Breskin LA, Khramtsova EA, Khramtsova G, Tsai PY, Fu YX, Abraham C, Turner JR. TNFR2 activates MLCK-dependent tight junction dysregulation to cause apoptosis-mediated barrier loss and experimental colitis. Gastroenterology 2013;145:407–415.

85. Rodriguez-Roisin R, Bartolome SD, Huchon G, Krowka MJ. Inflammatory bowel diseases, chronic liver diseases and the lung. Eur Respir J 2016;47:638–650.

86. Birukova AA, Zagranichnaya T, Fu P, Alekseeva E, Chen W, Jacobson JR, Birukov KG. Prostaglandins PGE(2) and PGI(2) promote endothelial barrier enhancement via PKA- and Epac1/Rap1-dependent Rac activation. Exp Cell Res 2007;313:2504–2520.

87. Le Faouder P, Baillif V, Spreadbury I, Motta JP, Rousset P, Chene G, Guigne C, Terce F, Vanner S, Vergnolle N, Bertrand-Michel J, Dubourdeau M, Cenac N. LC-MS/MS method for rapid and concomitant quantification of pro-inflammatory and pro-resolving polyunsaturated fatty acid metabolites. J Chromatogr B Analyt Technol Biomed Life Sci 2013;932:123–133.

88. Xia M, Zhu Y. Signaling pathways of ATP-induced PGE2 release in spinal cord astrocytes are EGFR trans-activation-dependent. Glia 2011;59:664–674.

89. Rolli-Derkinderen M, Toumaniantz G, Pacaud P, Loirand G. Rhoa phosphorylation induces Rac1 release from guanine dissociation inhibitor alpha and stimulation of vascular smooth muscle cell migration. Mol Cell Biol 2010;30:4786–4796.

90. De Quelen F, Chevalier J, Rolli-Derkinderen M, Mourot J, Neunlist M, Boudry G. N-3 polyunsaturated fatty acids in the maternal diet modify the postnatal development of nervous regulation of intestinal permeability in piglets. J Physiol 2011;589:4341–4352.